

Late Cretaceous topographic doming caused by initial upwelling of Deccan magmas: Stratigraphic and sedimentological evidence

Juan Li¹, Xiumian Hu^{1,†}, Eduardo Garzanti², Santanu Banerjee³, and Marcelle BouDagher-Fadel⁴

¹State Key Laboratory of Mineral Deposit Research, School of Earth Sciences and Engineering, Nanjing University, Nanjing 210023, China

²Laboratory for Provenance Studies, Department of Earth and Environmental Sciences, Università di Milano-Bicocca, 20126 Milano, Italy

³Department of Earth Sciences, Indian Institute of Technology Bombay, Powai, Mumbai 400076, India

⁴Department of Earth Sciences, University College London, London WC1H 0BT, UK

ABSTRACT

This study focused on uppermost Cretaceous sedimentary rocks deposited in the Himalayan region and around the core of peninsular India just before the eruption of the Deccan Traps. Detailed stratigraphic and sedimentological analysis of Late Cretaceous successions in the Himalayan Range together with literature data from the Kirthar fold-and-thrust belt and central to southeastern India document a marked shallowing-upward depositional trend that took place in the Campanian–Maastrichtian before the Deccan magmatic outburst around the Cretaceous–Tertiary boundary. Topographic uplift of the Indian peninsula began in Campanian time and is held responsible for thick sediment accumulation associated with shorter periods of nondeposition in peripheral areas (Himalayan Range, Kirthar fold belt, and Krishna-Godavari Basin) than in the central part of the Deccan Province. Surface uplift preceding Deccan volcanism took place at warm-humid equatorial latitudes, which may have led to an acceleration of silicate weathering, lowered atmospheric $p\text{CO}_2$, and climate cooling starting in the Campanian–Maastrichtian. The radial centrifugal fluvial drainage in India that is still observed today was established at that time.

INTRODUCTION

Large igneous provinces were emplaced on Earth's surface during a geologically short time span (Jerram and Widdowson, 2005; Bryan and Ernst, 2008) and were commonly fostered by the

ascent of so-called plumes originating either in the shallow or lower mantle (White and McKenzie, 1989; Anderson, 2013). It has been argued that a rising mantle plume could affect regions as wide as 2000 km, triggering a topographic uplift of the prevolcanic surface by up to more than 1 km (Cox, 1989; Rainbird and Ernst, 2001). Initial doming would have preceded the main phase of voluminous volcanism by as much as 20 m.y. (Campbell and Griffiths 1990; Sahu et al., 2013). The effects on sedimentary basins surrounding the uplifted region should be considerable and recognizable, thereby providing reliable evidence for locating ancient plume-related topographic domes. Such effects include thinning of strata onlapping onto the uplifted area, localized shoaling, occurrence of erosional unconformities, and radial paleocurrent patterns contrasting with those displayed by the underlying strata (Cox, 1989; Rainbird and Ernst, 2001).

The Deccan Traps, encompassing the Cretaceous–Tertiary boundary (ca. 66 Ma; Jay and Widdowson, 2008), is one of the most intensely studied large igneous provinces on Earth, generally considered as a classical example of plume-related uplift (Saunders et al., 2007). This scenario was challenged, however, by Sheth (2007), who emphasized instead posteruption uplift of the basaltic pile. The timing and magnitude of denudation inferred from fission-track-data modeling are largely dependent on the adopted assumptions (Gunnell et al., 2003), and sedimentary facies changes or unconformities have been ascribed alternatively to diverse autocyclic or allocyclic controls, including drainage diversions, climate changes, sea-level fluctuations, or local tectonic activity (Sharma, 2007).

In this article, we provide a stratigraphic and sedimentological analysis of sedimentary successions originally deposited during the latest Cretaceous along the Indian passive margin of the Neo-Tethys Ocean and now preserved in

the Tethys Himalayan zone of south Tibet in order to reconstruct the paleogeography of the northern Indian continental margin before the onset of the India-Asia continental collision. Combined with literature data from the Kirthar fold-and-thrust belt of western Pakistan and data from central and southeastern peninsular India (Fig. 1), we document the occurrence of widespread shallowing-upward depositional trends and of a prolonged stratigraphic hiatus, and we discuss the regional paleotectonic implications of stratigraphic data, which we relate to Deccan magmatic upwelling.

GEOLOGICAL SETTING

The Tethys Himalaya, stretching for ~1500 km from northwestern India to southern Tibet (Fig. 2A), is one of the major tectonic domains of the Himalayan orogen (Gansser, 1964). Its northern boundary coincides with the Indus-Yarlung suture, whereas the southern boundary is represented by the South Tibetan detachment system (Searle and Godin, 2003), the tectonic contact with the Greater Himalaya metamorphic unit. The Tethys Himalaya is traditionally subdivided into southern and northern zones separated by the Gyirong-Kangmar thrust (Ratschbacher et al., 1994). The southern zone consists of mostly shelfal carbonate and siliciclastic rocks of Paleozoic to Eocene age (Jadoul et al., 1998; Sciunnach and Garzanti, 2012), whereas the northern zone comprises Mesozoic to Paleocene deeper-water sediments.

During the earliest Cretaceous, the northern continental margin of India was situated at middle latitudes in the Southern Hemisphere (Huang et al., 2015), while the Lhasa block lay at low latitudes in the Northern Hemisphere. In the Early Cretaceous, India rifted from Gondwana and drifted northward (Garzanti, 1993a; Hu et al., 2010) to collide with the Asian active

[†]Corresponding author: huxm@nju.edu.cn.

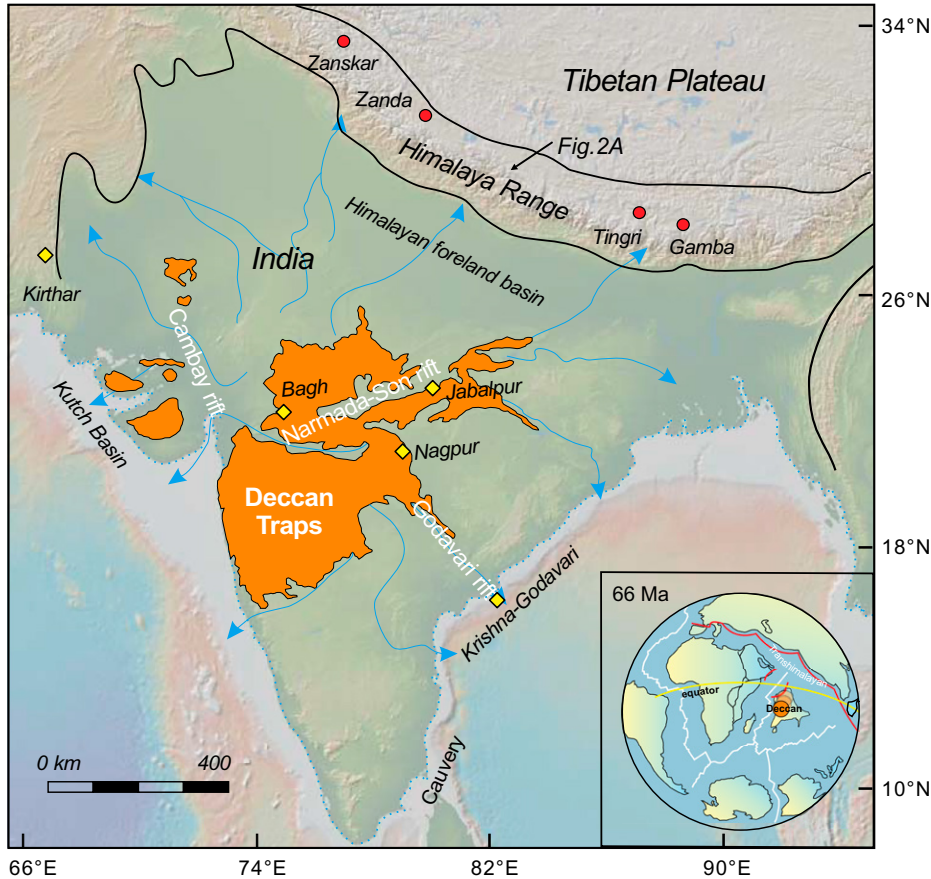


Figure 1. Map of peninsular India (modified after Garzanti and Hu, 2015) showing the Deccan flood basalt province, localities discussed in text, and drainage pattern (blue arrows) inferred to have originated in latest Cretaceous time (Cox, 1989). Red dots indicate locations of the stratigraphic logs shown in Figure 3, and yellow rhombuses indicate locations of the stratigraphic logs shown in Figure 11. Inset shows the location of the Indo-Tibetan region in the latest Cretaceous (after Stampfli and Borel, 2002).

continental margin in the middle Paleocene (Wu et al., 2014; DeCelles et al., 2014; Hu et al., 2016). Our three study areas are located in the southern Tethys Himalaya near the towns of Gamba, Tingri, and Zanda (Fig. 2), where a marine sedimentary succession ranging from the Upper Cretaceous to the Eocene is continuously exposed (Fig. 3).

SAMPLING AND METHODS

Samples were collected at stratigraphic intervals between 1 and 3 m in well-exposed Upper Cretaceous measured sections of the classic areas of Gamba (29 samples from the Jiubao section, 28°16'53.6"N, 88°31'10.2"E; 2B), Tingri (50 samples from the Gelamu section, 28.48°N, 87.04°E; Fig. 2C), and Zanda (58 samples from the Xiala section, 28.28°N, 88.52°E; Fig. 2D).

Biostratigraphic analysis was based on taxonomic determinations of Late Cretaceous planktonic foraminifera according to Premoli

Silva and Verga (2004). Despite the poor to moderate preservation of the specimens, key morphological characteristics such as coiling mode, peripheral shape, arrangement and number of chambers, presence or absence of keels, and sutural properties enabled us to construct a reliable biostratigraphy. Stratigraphic ranges were defined by the planktonic foraminifera (PF) zonal scheme of BouDagher-Fadel (2013), tied to the time scale of Gradstein et al. (2012) and developed from the calibration of the N-zonal scheme of Blow (1979) and the M-zonal scheme of Berggren (1973), further revised by Wade et al. (2011).

Microfacies analysis was performed by examining detrital minerals, macrofossil and microfossil assemblages, and textures as observed in both thin sections and outcrop. Macrofossil groups, including gastropods, echinoderms, larger, smaller, and agglutinated benthic foraminifera, and calcareous red and green algae, were identified using the descriptions and pho-

tographs in Flügel (2010), and these were used to determine the environment of deposition according to Wilson (1975) and Flügel (2010). Carbonate and mixed siliciclastic-carbonate rocks were classified based on Dunham (1962), Embry and Klovan (1971), and Mount (1985).

STRATIGRAPHY

In the Tingri and Gamba areas of the central southern Tethys Himalaya, the uppermost Cretaceous succession is subdivided into four stratigraphic units (from base to top: Gambacunkou, Jiubao, Zhepure Shanpo, and Jidula Formations; Garzanti and Hu, 2015; Fig. 3). Two stratigraphic units (Gucuocun and Bolinxiala Formations) are identified in the western Tethys Himalaya (Zanda area; Fig. 3).

Gamba

In the Gamba area, the Gambacunkou Formation consists of dark-gray marl and marly limestone deposited in late Albian to Santonian times (Willems and Zhang, 1993). The overlying 40-m-thick Jiubao Formation comprises mainly thin- to medium-bedded limestone and marly limestone yielding abundant planktonic foraminifera of Santonian to earliest Campanian age (Wan et al., 2002). The uncomfortably overlying 170-m-thick Zhepure Shanpo Formation (here commonly named with the local synonym Zongshan Formation) consists of marl and nodular marly limestone with reworked fossils intercalated with storm-surge turbidites in the lower 50 m (Fig. 4A). Limestones yielding calcareous algae and benthic foraminifera are interbedded with rudist biostromes and subordinate marls in the upper part of the unit (Wan et al., 2002). The overlying ~180-m-thick Jidula Formation consists of quartzose sandstones intercalated with black limestones in the middle part; a mudrock bed at the base yielded foraminifera of early Danian age (Wan et al., 2002).

Tingri

In the Tingri area, the 600-m-thick Gambacunkou Formation consists of gray marlstone and marly limestone with abundant planktonic foraminifera of late Albian to early Coniacian age (Willems et al., 1996; Wendler et al., 2009). The overlying 80-m-thick Jiubao Formation consists of marly limestone and limestone yielding planktonic foraminifera of early Coniacian to latest Santonian age (Wu et al., 2011; Hu et al., 2012). A paraconformity at the top of the unit is followed by the 190-m-thick Zhepure Shanpo Formation, which consists of mixed siliciclastic-carbonate rocks (Fig. 4B, C). Sand-

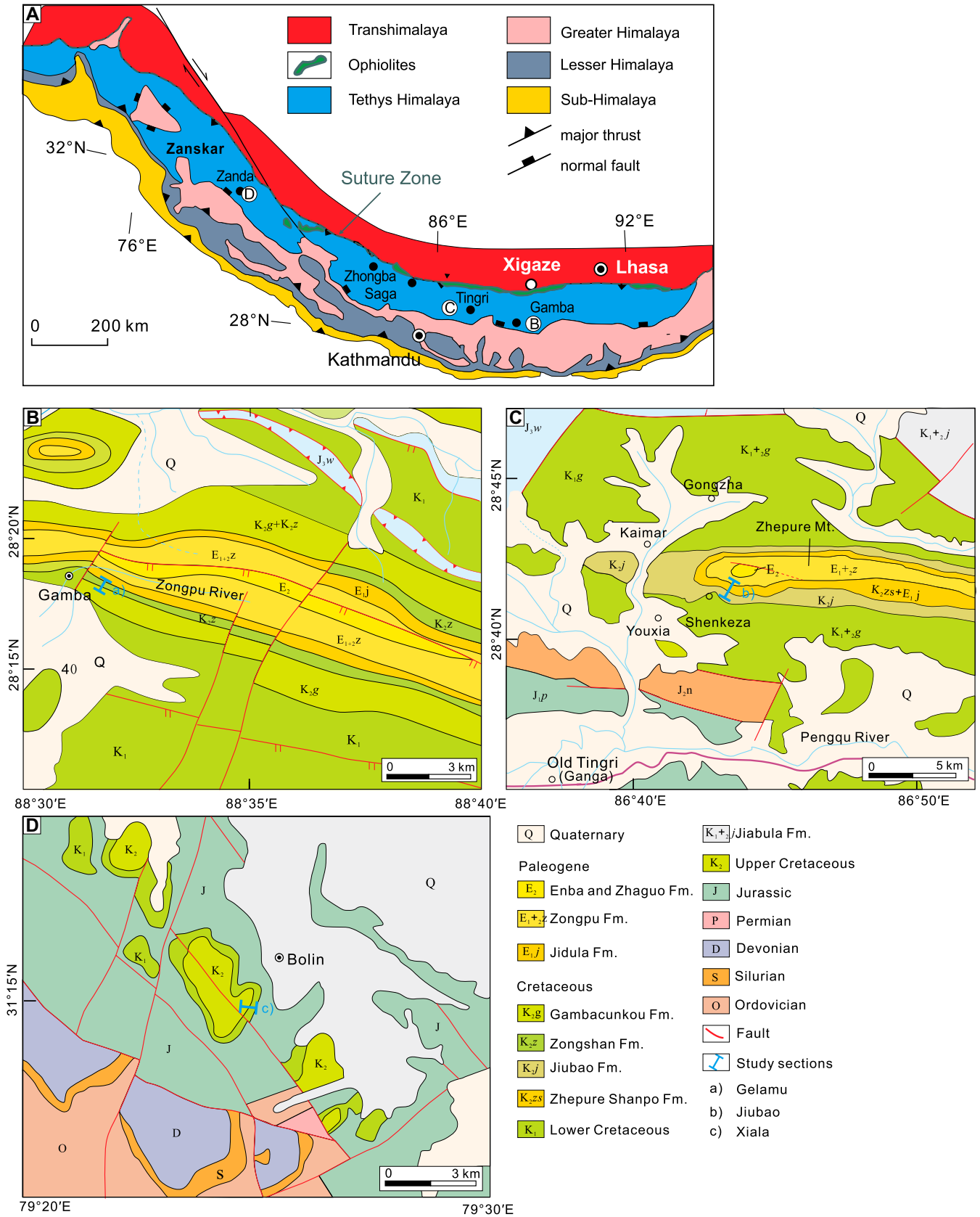


Figure 2. Geology and locations of measured stratigraphic sections in southern Tibet. (A) Sketch map of the Himalayan Range (after Pan et al., 2004); (B) Gamba; (C) Tingri; (D) Zanda.

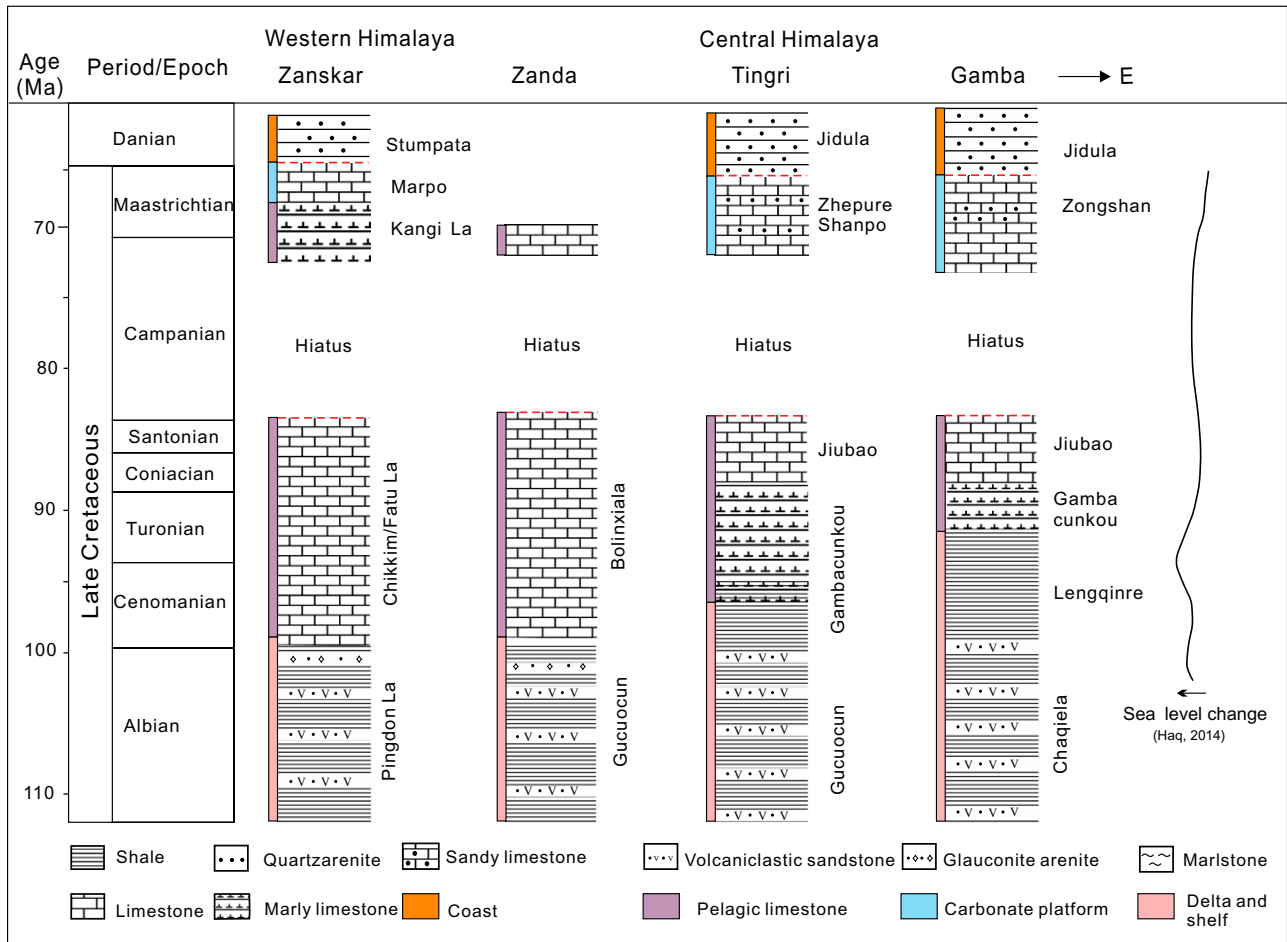


Figure 3. Correlation chart for Upper Cretaceous stratigraphic units of the Tethys Himalaya. Locations of the three sections measured in southern Tibet are indicated in Figure 2. Stratigraphic logs from the Zanskar Range in the western Tethys Himalaya are modified from Premoli Silva et al. (1991) and Garzanti (1993b).

stones are interpreted as storm-surge turbidites and become more frequent and coarser grained up section (Willems et al., 1996; Fig. 4D, E). Calcareous interbeds yielding reworked planktonic foraminifera of latest Campanian to early Maastrichtian age (Willems et al., 1996) are overlain by calcareous sandstone with gastropods, ostracods, and benthic foraminifera, capped in turn by sandstone, sandy limestone, and marl yielding planktonic foraminifera of Danian age (Wan et al., 2002). The overlying Jidula Formation (75 m thick) comprises calcareous quartzose sandstone with a shale interval in the middle, interbedded with marly nodular limestone with ferruginous nodules at the top yielding gastropods, ostracods, and a few foraminifera of early Danian age (Willems et al., 1996; Wan et al., 2002).

Zanda

The Gucucun Formation of the Zanda area, with type section near Lanong La in Nyalam

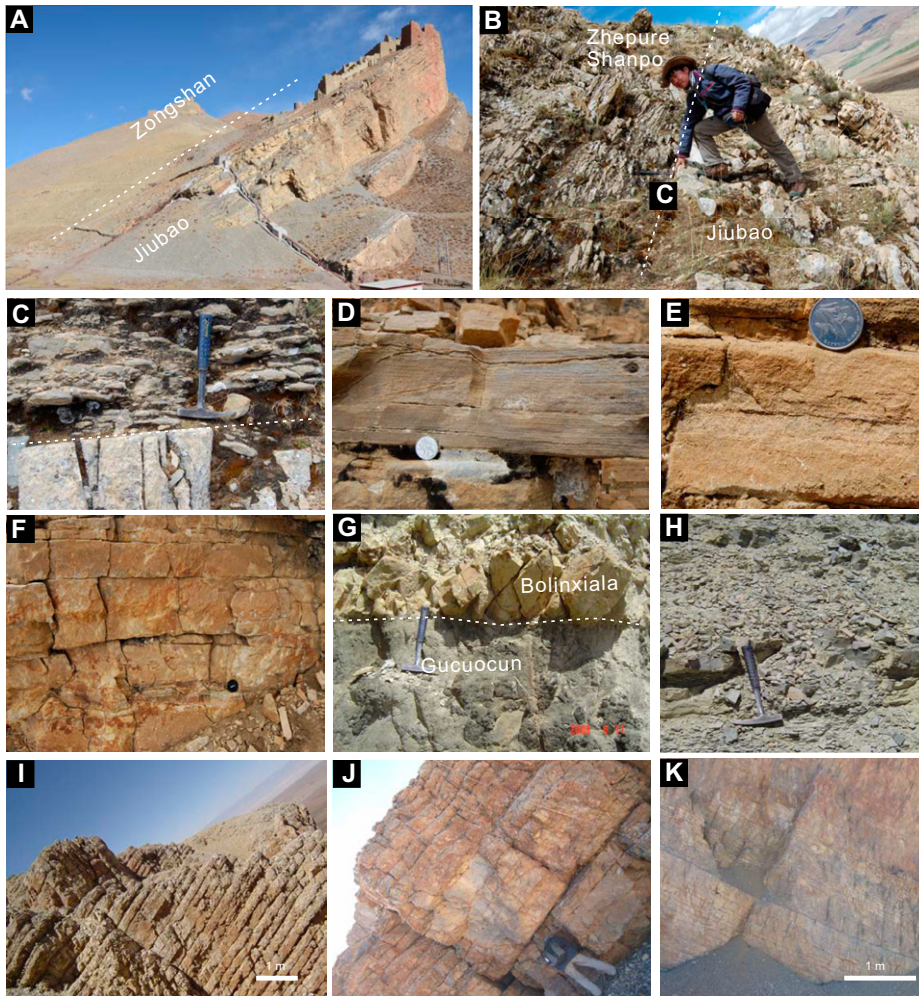
County (Yu et al., 1983), is equivalent to the Wölong Formation of Jadoul et al. (1998) and to the Giurnal Formation of the Spiti-Zanskar synclinorium (Garzanti, 1993b). It is 400 m thick and mainly consists of thin- to thick-bedded dark-gray and gray shale interbedded with volcaniclastic sandstone (Fig. 4G; Hu et al., 2017). Abundant ammonites and bivalves suggest a late Tithonian to Albian age for these prodelta to inner-shelf deposits (Hu et al., 2006). The overlying Bolinxiala Formation, named after the Xiala section in Zanda County (Guo et al., 1991), is equivalent to the Chikkim Formation of the Spiti-Zanskar synclinorium (Premoli Silva et al., 1991; Bertle and Suttner, 2005). It is 160 m thick and dominated by thin-bedded dark-gray limestone intercalated with marly limestone in the lower part, medium-bedded limestone in the middle part, and thick-bedded limestone intercalated with marly limestone in the upper part (Figs. 4H–4K). This pelagic unit yields abundant planktonic foraminifera together with calcispheres and radiolarians (Li et al., 2009).

BIOSTRATIGRAPHY

The biostratigraphy of the Jiubao and Zhepure Shanpo Formations in the Gelamu (Tingri) and Jiubao sections (Gamba) was described in detail in BouDagher-Fadel et al. (2015). Here, we focus specifically on the disconformable Jiubao–Zhepure Shanpo boundary in Tingri and Gamba (Figs. 5 and 6; Figs. DR1 and DR2¹), and on biostratigraphic features of the Bolinxiala Formation in Zanda (Fig. 7; Fig. DR3 [see footnote 1]).

In the Jiubao and Gelamu sections (Gamba and Tingri) the upper Jiubao Formation, *Dicarinella primitiva*, *Concavatotruncana concavata*, and *Contusotruncana fornicata* indicate a Coniacian age (89.8–86.3 Ma), and

¹GSA Data Repository item 2019300, Figures DR1–DR3, is available at <http://www.geosociety.org/datarepository/2019> or by request to editing@geosociety.org.



Formation, followed by *Contusotruncana wal-fishensis* and *Plummerita hantkeninoides* indicating the earliest Maastrichtian in the upper of the Bolinxiala Formation (Fig. 7; Fig. DR3 [footnote 1]).

MICROFACIES ANALYSIS

The purpose of the microfacies analysis was to integrate sedimentological and paleontological results in order to evaluate the depositional evolution during the latest Cretaceous and specifically across the Jiubao–Zhepure Shanpo boundary. We identified 10 microfacies (MF) types corresponding to outer-ramp to inner-ramp environments (Table 1).

Outer-Ramp to Middle-Ramp (MF1–MF5) Environments

MF1 Mudstone

Dark-gray marly limestones of the lowermost Bolinxiala Formation (Fig. 4H) are characterized by locally laminated micritic matrix encasing a few planktonic foraminifera, calcispheres, and pyrite crystals (Fig. 8A). Texture and fossil content indicate deposition below storm wave base (SWB) in a proximal outer-ramp setting. MF1 is equivalent to the standard microfacies (SMF) 3 or RMF5 of Flügel (2010).

MF2 Small Calcisphere Wackestone

Dark-gray marly limestones common in the lower part of Bolinxiala formation (Fig. 4H) are wackestones with small calcispheres (5%–10% of the rock, 30–50 μm in diameter), minor planktonic foraminifera (Fig. 8B), and thin-shelled bivalves. Micritic matrix and faunal content indicate a low-energy outer-ramp to middle-ramp environment. MF2 is considered equivalent to SMF3 or RMF5 of Flügel (2010).

MF3 Thin-Shelled Bivalve Wackestone

Thin- to medium-bedded gray limestones in the lower part of the Bolinxiala Formation (Fig. 4H) contain abundant thin-shelled bivalves, small calcispheres, planktonic foraminifera (Fig. 8C), and minor ostracods and echinoderm fragments. Micritic matrix is locally recrystallized to microspar. Textural properties and faunal content point to deposition below SWB, in low-energy outer-ramp settings (Flügel, 2010).

MF4 Microbioclastic–Planktonic Foraminiferal Wackestone

Medium- to thick-bedded limestones common in the middle part of Bolinxiala Formation and in the Jiubao Formation at Gamba

Figure 4. Outcrop photographs, showing unconformable contact between the Jiubao and Zongshan (Zhepure Shanpo) Formation in the Gamba (A) and Tingri (B, C) areas; parallel lamination (D), graded bedding (E), and pinching out (F) in Zhepure Shanpo sandstones; depositional contact between the Gucuocun and overlying Bolinxiala Formations (G), alternating thin-bedded and marly limestones (lower Bolinxiala Formation) (H); medium- to thick-bedded limestones (middle Bolinxiala Formation) (I); medium- to thick-bedded limestones intercalated with marly limestones (upper Bolinxiala Formation) (J); and thin- to thick-bedded limestones (uppermost of Bolinxiala Formation) (K).

Concavototruncana asymetrica points to a latest Santonian age for the uppermost (86.3–83.6 Ma; Figs. 5 and 6; Figs. DR1 and DR2 [footnote 1]). In the lower Zhepure Shanpo Formation, *Globotruncanita stuartiformis* and *Radotruncana subspinosa* suggest a late Campanian age, followed by the appearance of *Globotruncanita stuarti*, *Globotruncanita conica*, and *Kuglerina rotundata* indicating an early to middle Maastrichtian age, then *Globotruncana arca*, *Globotruncanita stuarti*, *Abathomphalus mayaroensis*, *Kuglerina rotundata*, *Globotruncanita conica*, and *Racemiguembelina intermedia* indicating a late Maastrichtian age (67–66 Ma; Figs. 5 and 6; Figs. DR1 and DR2 [footnote 1]).

In the Xiala section (Zanda), the assemblage of *Rotalipora appenninica*, *Rotalipora montsalvensis*, *Thalmanninella micheli*, and *Rotalipora cushmani* indicates a middle to late Cenomanian age for the lowermost Bolinxiala Formation. The assemblage of *Marginotruncana* and *Sigalittruncana biconvexiformis* indicates the Turonian, *Contusotruncana fornicata* indicates the Coniacian, and *Concavototruncana asymetrica* indicates a Santonian age for the lower Bolinxiala Formation (Fig. DR3 [footnote 1]). Then the foraminiferal assemblage sharply changes upward to *Globotruncanella havanensis*, *Globotruncana aegyptiaca*, and *Gansserina gansseri*, indicating the late Campanian for the middle of Bolinxiala

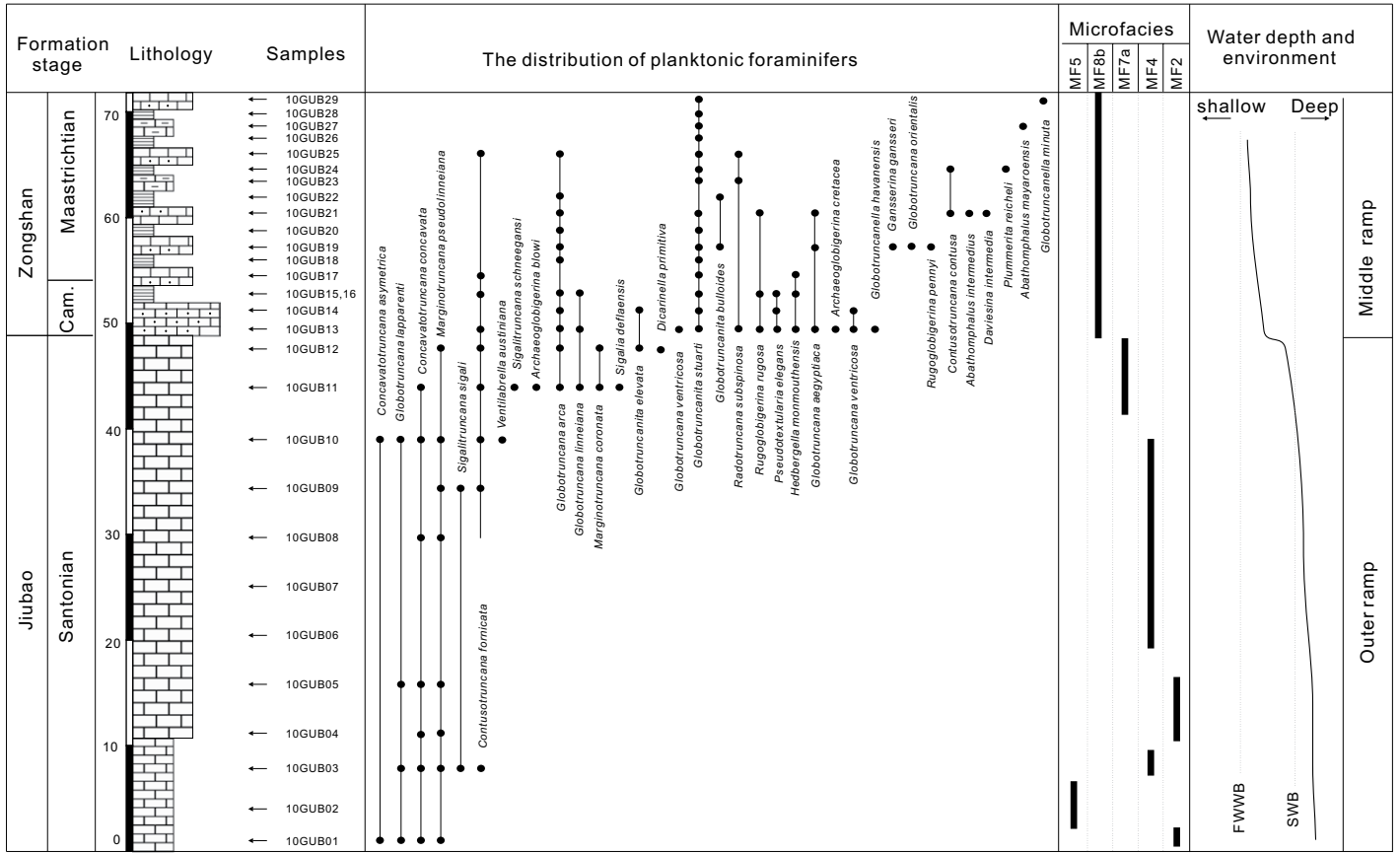


Figure 5. Lithological log of the Jiubao section (Gamba area) showing the distribution of planktonic foraminifera, carbonate microfacies, interpreted paleowater depths, and sedimentary environments for the upper Jiubao to lower Zhepure Shanpo Formations. Cam—Campanian; FWFB—fair-weather wave base; SWB—storm wave base.

(Figs. 4A and 4I) are evenly bedded mudstones and wackestone with abundant micro-bioclots and planktonic foraminifera (Fig. 8D), associated with small calcispheres, textulariids, mostly siliceous sponge spicules, thin-shelled bivalves, ostracods, and echinoderm fragments. Micritic matrix is locally recrystallized to microspar. Bioclots are inferred to have been transported from shallower environments during storms. Deposition in an outer-ramp to middle-ramp environment between fair-weather wave base (FWFB) and SWB is indicated by texture and faunal content (Flügel, 2010).

MF5 Peloidal Grainstone

MF5 is uncommon and only observed in the Jiubao Formation at Gamba, where it is locally intercalated with MF2. Abundant fine- to medium-sand-sized, well-sorted peloids and minor micro-bioclots inferred as transported seaward during storms are set in sparitic cement (Fig. 8E). Deposition in an outer-ramp to middle-ramp environment between FWFB and SWB is inferred (Flügel, 2010).

Middle Ramp (MF6–MF8) Environments

MF6 Intra-bioclotal Packstone

Thin-bedded gray limestones found in the lowermost Zhepure Shanpo Formation contain abundant bioclots (planktonic foraminifera and minor small hyaline benthic foraminifera, echinoderms, and ostracods) and intraclasts (Figs. 8F–8H). Mixed benthic and planktonic biota and abundant reworked intraclasts suggest storm deposition below the FWFB (microfacies SMF4 or RMF9 of Flügel, 2010).

MF7a Planktonic Foraminiferal Wackestone

MF7a, occurring in the upper Jiubao Formation at Gamba and in the middle Bolinxiala Formation, is characterized by micritic matrix encasing common planktonic foraminifera and calcispheres, along with minor hyaline benthic foraminifera, ostracods, mollusk fragments, and echinoderms (Fig. 9A). Benthic foraminifera increase up section, suggesting a shallowing-upward trend. MF7a is inferred to have been deposited between FWFB and SWB in a middle-ramp setting (Flügel, 2010).

MF7b Sandy Planktonic Foraminiferal Packstone

Thin- to medium-bedded gray sandy limestones of the lower Zhepure Shanpo Formation at Tingri have the same faunal composition and content of MF7a, but much greater amounts and coarser size of terrigenous quartz grains (Figs. 9B and 9C). Abundant planktonic foraminifera with chambers commonly filled with ferrous minerals (most probably pyrite) are associated with small hyaline and agglutinated benthic foraminifera, minor calcispheres, ostracods, and echinoderm fragments. MF7b is inferred to indicate deposition below FWFB, in low-energy settings with sporadic siliciclastic supply (Flügel, 2010).

MF8a Calcisphere Grainstone-Packstone

Thin-bedded gray limestones in the upper Bolinxiala Formation mostly include calcispheres and planktonic foraminifera (≤90% of the rock), associated with small benthic foraminifera, echinoderm fragments, and other bioclots. Micrite or locally sparitic cement occurs (Fig. 9D). Planktonic foraminifera decrease up

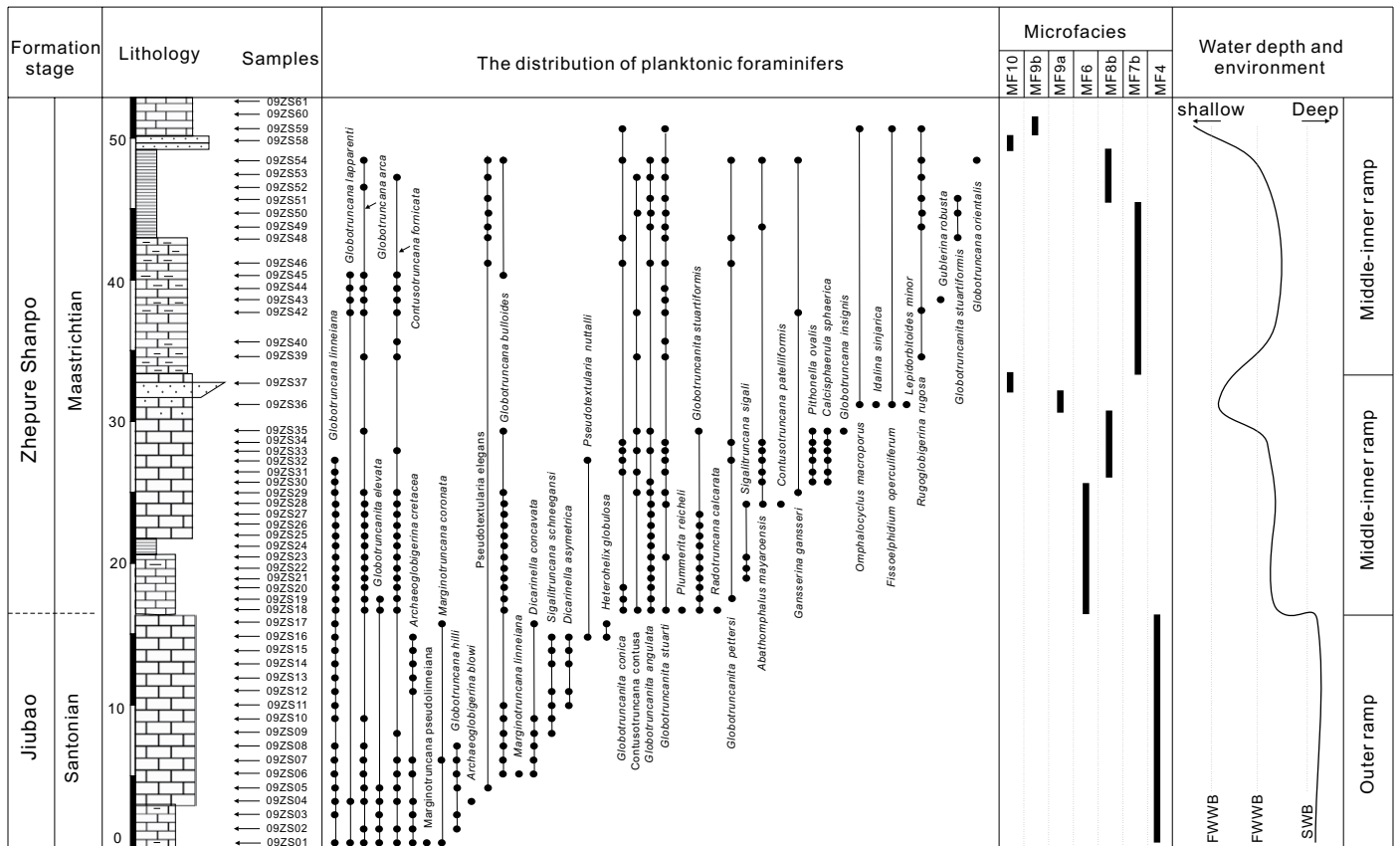


Figure 6. Lithological log of the Gelamu section (Tingri area) showing the distribution of planktonic foraminifera, carbonate microfacies, interpreted paleowater depths, and sedimentary environments for the upper Jiubao to lower Zhepure Shanpo Formations. FWWB—fair-weather wave base; SWB—storm wave base.

section in abundance. Calcspheres, larger than in MF2 and mostly representing dinoflagellates, suggest offshore deposition from suspension in high-productivity and nutrient-rich conditions (Wendler et al., 2002). A middle-ramp environment below FWWB and slightly shallower than for MF7a is indicated (Flügel, 2010).

MF8b Sandy Calcsphere Packstone

Thin- to medium-bedded gray limestones found in the lower Zongshan Formation mostly contain calcspheres and planktonic foraminifera (Fig. 9E), together with minor ostracods, small benthic foraminifera, and echinoderm fragments set in micritic matrix. Silt-sized quartz grains reaching 5% in abundance characterize MF8b, which was deposited on a middle ramp with sporadic siliciclastic supply (Flügel, 2010).

Inner Ramp (MF9–MF10) Environments

MF9a Bioclastic Packstone

Gray bioclastic packstone in the upper Zhepure Shanpo Formation at Tingri contains abundant macrofossils and microfossils set in micritic

matrix (Fig. 9F). Highly diversified, large hyaline benthic foraminifera include *Lepidorbitoides*, *Siderolites*, and *Rotalia*. Abundant uncoiled agglutinated benthic foraminifera and coralline algae are associated with echinoderm plates and spines, bivalves, and rare planktonic foraminifera. Intraclasts of calcsphere packstone eroded from underlying strata and quartz grains are common. Rock-forming large benthic foraminifera and calcareous red algae typical of the photic zone and platform-margin settings indicate inner-ramp environments above the FWWB and restricted to open-marine conditions for MF9a (equivalent to SMF18-FOR and RMF 13 of Flügel, 2010).

MF9b Sandy Bioclastic Floatstone/Bioclastic Sandstone

The uppermost Zhepure Shanpo Formation at Tingri is rich in silt-sized quartz grains set in micritic matrix. Abundant agglutinated or larger benthic foraminifera and calcareous red algae are associated with planktonic foraminifera and echinoderm spines (Fig. 9G). Common detrital quartz indicates a slightly shallower depositional environment than for MF9a (Flügel, 2010).

MF10 Quartzose Sandstone

Fine- to medium-sand-sized, well-sorted, subrounded, and quartz-cemented quartz grains are associated with minor lithic fragments and detrital zircon in sandstones of the Zhepure Shanpo Formation (Fig. 9H). Sedimentary structures, including erosional base, graded bedding, and planar oblique or parallel lamination (Figs. 4D and 4E), suggest deposition on the inner shelf by hyperpycnal flows or storm-surge turbidites.

LATE CRETACEOUS SEDIMENTARY EVOLUTION IN THE TETHYS HIMALAYA

Facies and microfacies analyses indicate that the Indian passive margin facing the Neo-Tethys evolved from outer ramp, to middle ramp, and inner ramp environments during the Late Cretaceous (Figs. 5–7, and 10).

Gamba

The boundary between the upper Jiubao and lower Zhepure Shanpo (Zongshan) Formations documents a sharp change from

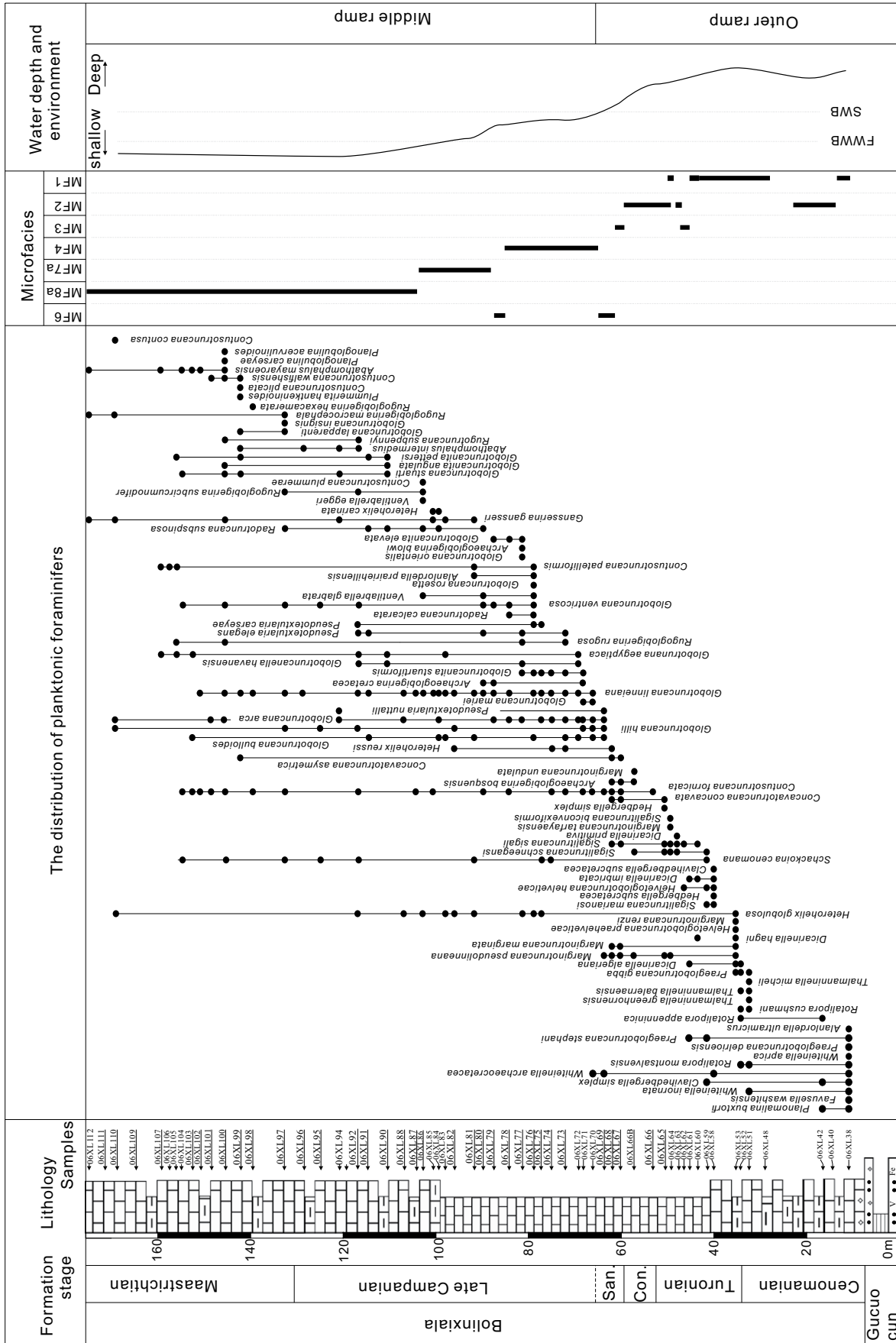


Figure 7. Lithological log of the Bolinxiala Formation, showing the distribution of planktonic foraminifera, carbonate microfacies, interpreted paleowater depths, and sedimentary environments. Con—Coniacian; San—Santonian; MF—microfacies; FWB—fair-weather wave base; SWB—storm wave base.

TABLE 1. DESCRIPTION AND ENVIRONMENTAL INTERPRETATION OF THE 10 IDENTIFIED MICROFACIES

Microfacies	Planktonic foraminifera	Carbonate grains				Groundmass		Terrigenous grains (percentage, size range)	Sedimentary structures	Standard microfacies (Flügel, 2010)	Depositional environment
		Calcisphere (percentage, diameter range)	Peloids	Bioclasts	Bivalves	Intraclasts	Matrix				
MF1	Mudstone	3	1	—	—	—	96	—	Planar lamination	RMF5	Low-energy outer ramp, below SWB
MF2	Small calcisphere wackestone	2	10 (0.03–0.05 mm)	—	1	—	87	—	—	RMF6	Low-energy outer ramp, below SWB
MF3	Thin-shelled bivalve wackestone	3	5	—	15	—	77	—	—	RMF5	Low-energy outer ramp, below SWB
MF4	Microbioclastic–planktonic foraminiferal wackestone	3	2	25	1	—	70	—	Burrows	RMF3	Low-energy outer-middle ramp, influenced by SWB
MF5	Peloidal grainstone	—	—	30	3	—	10	57	—	RMF4	Low-energy outer ramp, storm deposits
MF6	Intrabioclastic packstone	10	—	45	—	15	27	—	Bioturbation	RMF9	Middle ramp, between FWWB and SWB
MF7a	Planktonic foraminiferal wackestone	15	—	5	—	—	80	—	—	RMF5	Middle ramp, between FWWB and SWB
MF7b	Sandy planktonic foraminiferal wackestone	25	—	10	—	—	65	—	Bioturbation	RMF5	Middle ramp influenced by terrigenous, between FWWB and SWB
MF8a	Calcisphere grainstone-packstone	5	75 (0.1–0.15 mm)	—	—	—	20	—	—	RMF27	Middle ramp, between FWWB and SWB
MF8b	Sandy calcisphere packstone	5	20 (0.1–0.15 mm)	25	—	—	45	5 (0.02–0.05 mm)	—	RMF27	Middle ramp influenced by terrigenous, between FWWB and SWB
MF9a	Bioclastic packstone	—	—	60	—	10	5	15	—	RMF13	Inner ramp, open marine above FWWB
MF9b	Sandy bioclastic floatstone/bioclastic sandstone	—	—	25	—	15	35	15 (0.1–0.3 mm)	—	RMF13	Inner ramp, open marine above FWWB
MF10	Quartzose sandstone	—	—	—	—	—	11	89 (0.1–0.4 mm)	Graded bedding, parallel lamination	—	Inner ramp, high-energy storm deposits, above FWWB

Note: FWWB—fair-weather wave base; SWB—storm wave base.

pelagic to shelfal and platform-margin conditions (Fig. 5). Microfacies in the uppermost Jiubao Formation (microbioclastic–planktonic foraminiferal wackestone [MF4] and minor small calcisphere wackestone [MF2], peloidal grainstone [MF5], and thin-shelled bivalve wackestone [MF3]) document deposition in an outer-ramp environment, whereas planktonic foraminiferal wackestone (MF7a) and sandy calcisphere packstone (MF8b) mark the abrupt transition to much shallower middle-ramp environments in the lowermost Zhepure Shanpo Formation. Microfacies analysis allowed us to estimate a corresponding major change in paleowater depth, from 300–400 m for the topmost Jiubao Formation to 200–300 m for the base of the Zhepure Shanpo Formation (Leckie, 1987; Premoli Silva and Sliter, 1999).

Tingri

The same paleoenvironmental changes observed in the Gamba area are documented at Tingri (Fig. 6). Deposition of microbioclastic–planktonic foraminiferal wackestone (MF4) in an outer-ramp environment at the top of the Jiubao Formation was abruptly replaced by intrabioclastic packstone (MF6), documenting a shallower middle-ramp environment at the base of the Zhepure Shanpo Formation.

The overlying sedimentary succession also documents a similar paleoenvironmental trend. Sandy calcisphere packstones (MF8b) that accumulated on a middle ramp are overlain by bioclastic packstones (MF9a) deposited in open-marine conditions on an inner ramp, capped in turn by quartzose sandstones (MF10). The second succession starts with planktonic foraminiferal packstones including quartz grains (MF7b) deposited on a middle ramp, passing upward to calcisphere packstones (MF8a), suggesting shallower shelf environments, and then to quartzose sandstones (MF10) and sandy bioclastic floatstones (MF9b) deposited on an inner ramp in open-marine conditions. Increasing terrigenous supply and progressive shallowing through time are indicated (Fig. 6).

Zanda

Carbonate microfacies indicate a transition from outer-ramp to middle-ramp environments throughout the Bolinxiala Formation, documenting a shallowing-upward trend (Fig. 7). Unlike the Tingri and Gamba areas, terrigenous detritus is lacking.

The lower to middle Bolinxiala Formation of middle Cenomanian to Santonian age consists of mudstone (MF1), small calcisphere packstone (MF2), and minor thin-shelled bivalve

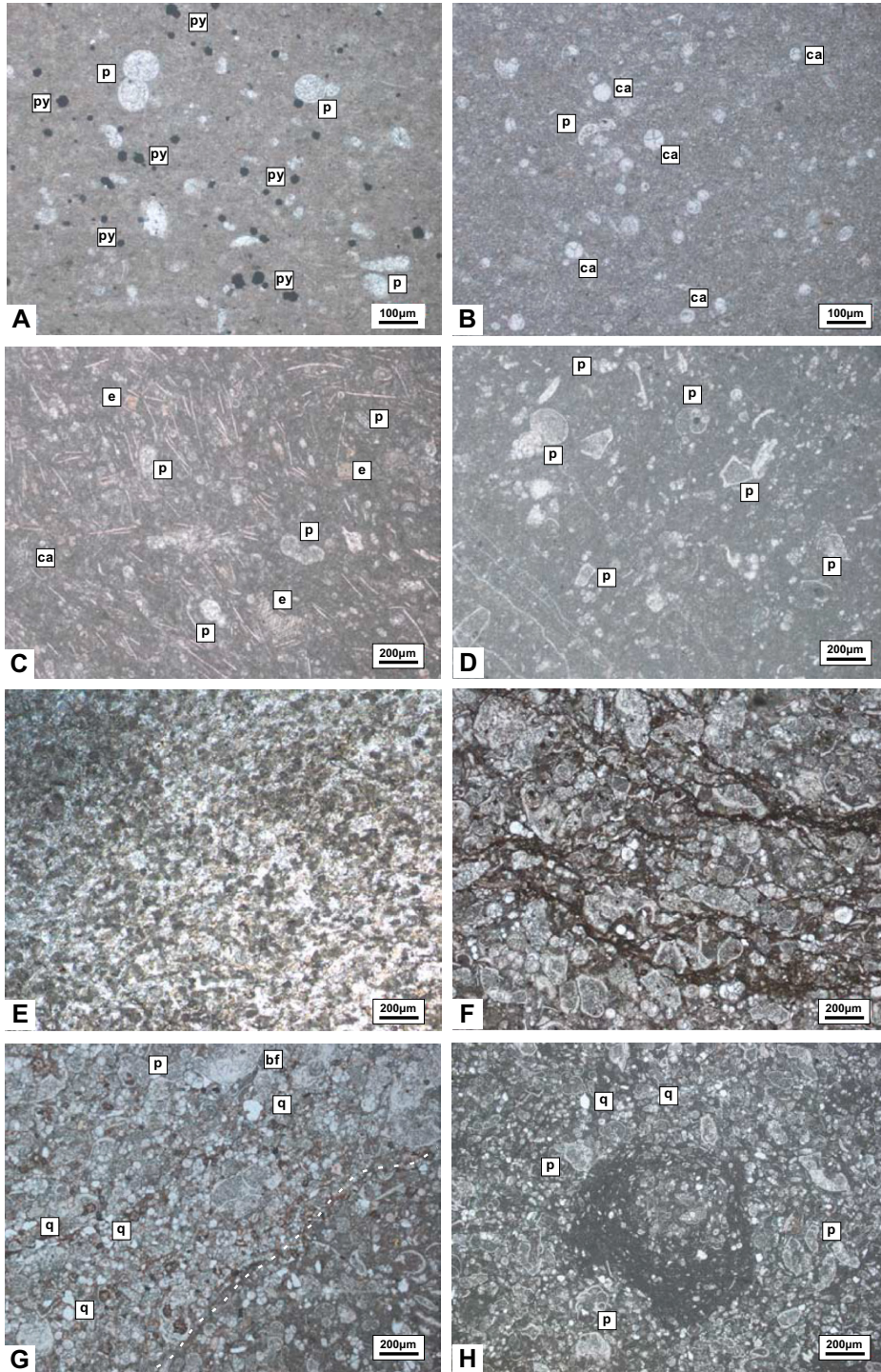


Figure 8. Microfacies MF1–MF6. (A) Mudstone with small planktonic foraminifera and pyrite (MF1). (B) Small calcisphere wackestone (MF2). (C) Thin-shelled bivalve wackestone (MF3). (D) Microbioclastic–planktonic foraminiferal wackestone (MF4). (E) Peloidal grainstone (MF5). (F) Bio-intraclastic packstone (MF6). (G) Erosive contact (MF6). (H) Bio-turbation (MF6). Abbreviations: bf—benthic foraminifer; ca—calcisphere; e—echinoid; p—planktonic foraminifer; py—pyrite; q—quartz.

wackestone (MF3), indicating deposition on an outer ramp. The sharply overlying intraclastic packstone (MF6) indicates a sudden shift

to middle-ramp environments dominated by planktonic foraminiferal wackestone (MF7a) and finally by calcisphere packstone (MF8a).

SEDIMENTATION AND DRAINAGE PATTERNS AROUND DECCAN-RELATED DOMAL UPLIFT

Advocates of mantle plumes have considered the Deccan province to be a classical example of plume-related uplift, and they have ascribed the response of adjacent sedimentary basins and catchment areas to dynamic uplift caused by mantle upwelling (Saunders et al., 2007). In this part of the article, we shall briefly describe the stratigraphic successions deposited around the core of peninsular India in order to investigate the potential effects of Deccan-related magmatic upwelling on sedimentation patterns.

Tethys Himalaya

The top of the Jiubao Formation is dated as the latest Santonian *Dicarinella asymetrica* zone (ca. 84 Ma; Figs. DR1, and DR2 [footnote 1]), whereas planktonic foraminifera at the base of the Zhepure Shanpo Formation indicate the latest Campanian (ca. 72 Ma; Figs. DR1 and DR2 [footnote 1]; Wu et al., 2011). Therefore, most of the Campanian is missing, and the disconformity between these two formations represents a hiatus of up to 12 m.y. The Campanian unconformity, well documented also in the Zanskar Range of the northwestern Himalaya (Premoli Silva et al., 1991), testifies to a major, widespread, broadly synchronous event along the Tethys Himalaya, interpreted as possibly related to the dynamic impact of magmatic upwelling at the base of the lithosphere (Hu et al., 2012; Garzanti and Hu, 2015). The marked decrease in water depth inferred between the top of the Jiubao Formation and the base of the Zhepure Shanpo Formation does not correspond to any significant sea-level fall in the global eustatic curve (Haq, 2014). This suggests a surface uplift of the order of ~100 m, which is compatible with the amount of topographic uplift usually observed in large continental igneous provinces (Saunders et al., 2007).

The Maastrichtian succession of the Zanskar Range testifies to the rapid transition from deep-water strata rich in deeper-dwelling planktonic foraminifera to shelfal faunas becoming more abundant up section in the Kangi La Formation (Fig. 3; Premoli Silva et al., 1991). The shallowing-upward trend with progressive increase in siliciclastic supply and accumulation rates during the Maastrichtian was followed by the progradation of a shallow-water carbonate ramp capped by shoreline quartzose sandstones in the Danian (Nicora et al., 1987). Felsitic volcanic rock fragments and detrital Cr-spinels with geochemical fingerprint

Kirthar Fold-and-Thrust Belt

The uppermost Cretaceous succession originally deposited along the western passive margin of India and presently exposed in the Kirthar range of western Pakistan (Fig. 1; Smewing et al., 2002; Kassi et al., 2009) is represented by the lower Campanian pelagic Parh Limestone, deposited at water depths exceeding 200 m, which was abruptly replaced by Upper Campanian to Maastrichtian shelfal sandstones of the Mughal Kot and Pab Formations (Fig. 11; Kazmi and Abbasi, 2008; Umar et al., 2011). The marked decrease in water depth from the Parh Formation to the Mughal Kot and Pab Formations does not correspond to any significant sea-level fall in the global eustatic curve (Haq, 2014) and thus suggests surface uplift. In the central Kirthar subbasin, the shelfal succession testifies to a clear shoaling trend from the Mughal Kot to the Pab Formation, documented by sand bodies increasing up section in grain size, bed thickness, and frequency of hummocky bed forms. In the southern Kirthar subbasin, the Mughal Kot Formation comprises basin-floor lobes, channel-fill sand bodies, and base-of-slope mud-rich lobes, whereas the overlying Pab Formation is dominated by slope-fan lobes and channel-levee deposits. The marked increase in siliciclastic influx from the Mughal Kot to the Pab Formation took place in the Campanian and has been related to uplift of the Indian Shield as it passed over the Reunion hot spot (Smewing et al., 2002; Kassi et al., 2009; Umar et al., 2011). The petrographic and geochemical composition of Pab sediments testifies to volcanoclastic supply from the Deccan Traps and intense chemical weathering in warm humid source areas located in continental India (Umar et al., 2014).

Central India (Main Deccan Province)

In central India, the Late Cretaceous sedimentary units resting either on Precambrian basement or Paleozoic Gondwanan strata and overlain by the Deccan Traps are mostly exposed as discontinuous patches a few to tens of square kilometers in area (Tandon, 2002). In the western Narmada valley (Bagh area), the Lower Cretaceous Nimar Sandstone is overlain by nodular or coralline limestones of Albian–Turonian age (Fig. 11; Tripathi, 2006). After a distinct hiatus spanning the Santonian and Campanian, sedimentation resumed during the Maastrichtian with deposition of glauconitic sandstone (Lameta Formation; Bansal et al., 2018). This hiatus corresponded to a period of global sea-level rise, indicating that NW

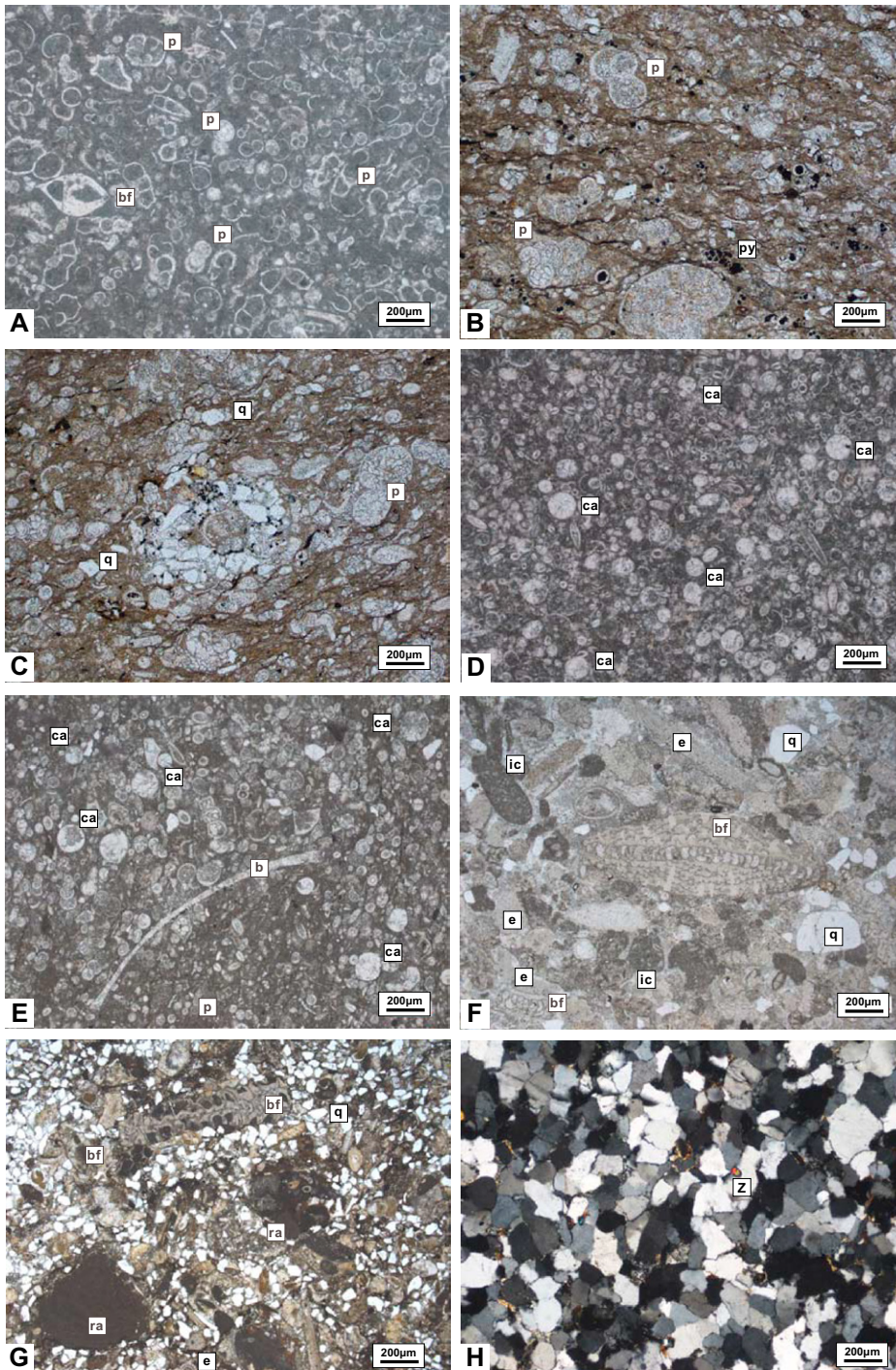


Figure 9. Microfacies MF7a–MF10. (A) planktonic foraminiferal wackestone (MF7a); (B) sandy planktonic foraminiferal packstone (MF7b); (C) bioturbation (MF7b); (D) calcisphere packstone (MF8a); (E) sandy calcisphere packstone (MF8b); (F) bioclastic packstone (MF9a); (G) sandy bioclastic floatstone (MF9b); (H) quartzose sandstone (MF10). Abbreviations: b—bivalve; bf—benthic foraminifer; ca—calcisphere; e—echinoid; ic—intraclast; p—planktonic foraminifer; py—pyrite; q—quartz; ra—red alga; z—zircon.

similar to Deccan spinels occur throughout Maastrichtian to Danian Tethys Himalayan sandstones. Notwithstanding the combined effect of subequatorial weathering and subse-

quent diagenesis, they testify that detritus from Deccan continental flood basalts reached well into the Indian passive margin (Garzanti and Hu, 2015).

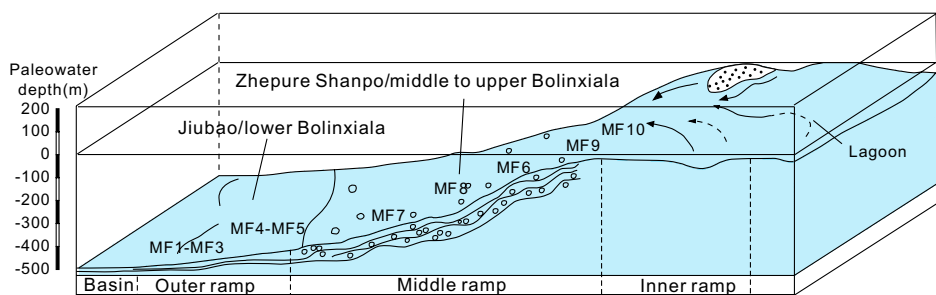


Figure 10. Sedimentary model for the Tethys Himalaya during the Late Cretaceous, indicating the relative paleogeographic position of microfacies types identified according to the depositional model of Flügel (2010).

India was undergoing significant tectonic uplift at this time. In the eastern Narmada valley (Jabalpur area), the Lower Cretaceous fluvial Jabalpur Sandstone is overlain by ephemeral braided-stream deposits of Maastrichtian age, passing upward to palustrine carbonates with multiple calcrete profiles capped in turn by locally channelized sheet-flood deposits (Tandon, 2002; Srivastava and Mankar, 2015). In the Nagpur area (Dongargaon basin), lacustrine sediments rest nonconformably on Precambrian basement and are overlain by dominant floodplain deposits encasing sparse fluvial channels (Tandon, 2000).

Southeastern India

During the Early Cretaceous rifting of India from Antarctica, the Krishna-Godavari Basin was tilted eastward and southeastward as part of the eastern passive margin of India (Gupta, 2006). The Cenomanian to Lower Maastrichtian Raghavapuram Shale, deposited in a low-energy shallow sea (Rao, 2001; Gupta, 2006), is unconformably overlain by coarse fluvial sediments of the Tirupati Formation, deposited at early to late Maastrichtian times (Fig. 11; Manmohan et al., 2003; Gupta, 2006). Major terrigenous supply and a threefold to fivefold

increase in accumulation rates, together with subsidence analysis of well-log data, suggest several hundred meters of transient surface uplift in late Campanian to early Maastrichtian times (Halkett et al., 2001). This is consistent with the pulse of exhumation revealed by thermal-history models based on apatite fission-track data in the Krishna and Godavari drainage basins, indicating accelerated cooling in the Campanian (Sahu et al., 2013).

Oblique lamination in the Tirupati Formation indicates southeastward paleocurrent directions (Rao, 2001), documenting a prominent provenance change with respect to the underlying Paleozoic and Lower Cretaceous strata, when sediment transport was toward the northwest. Sediment transport from uplifted basement in the northwest has persisted until today in the modern Krishna and Godavari River systems (Manmohan et al., 2003). Relatively rapid establishment of southeastward sediment transport with sudden influx of coarse detritus and the transition from marine to fluvial deposition strongly support the notion that the radial drainage pattern in the Indian peninsula initiated by topographic doming preceding the outburst of Deccan lavas, as advocated by Cox (1989).

Topographic doming related to mantle upwelling causes shoaling and thinning of strata

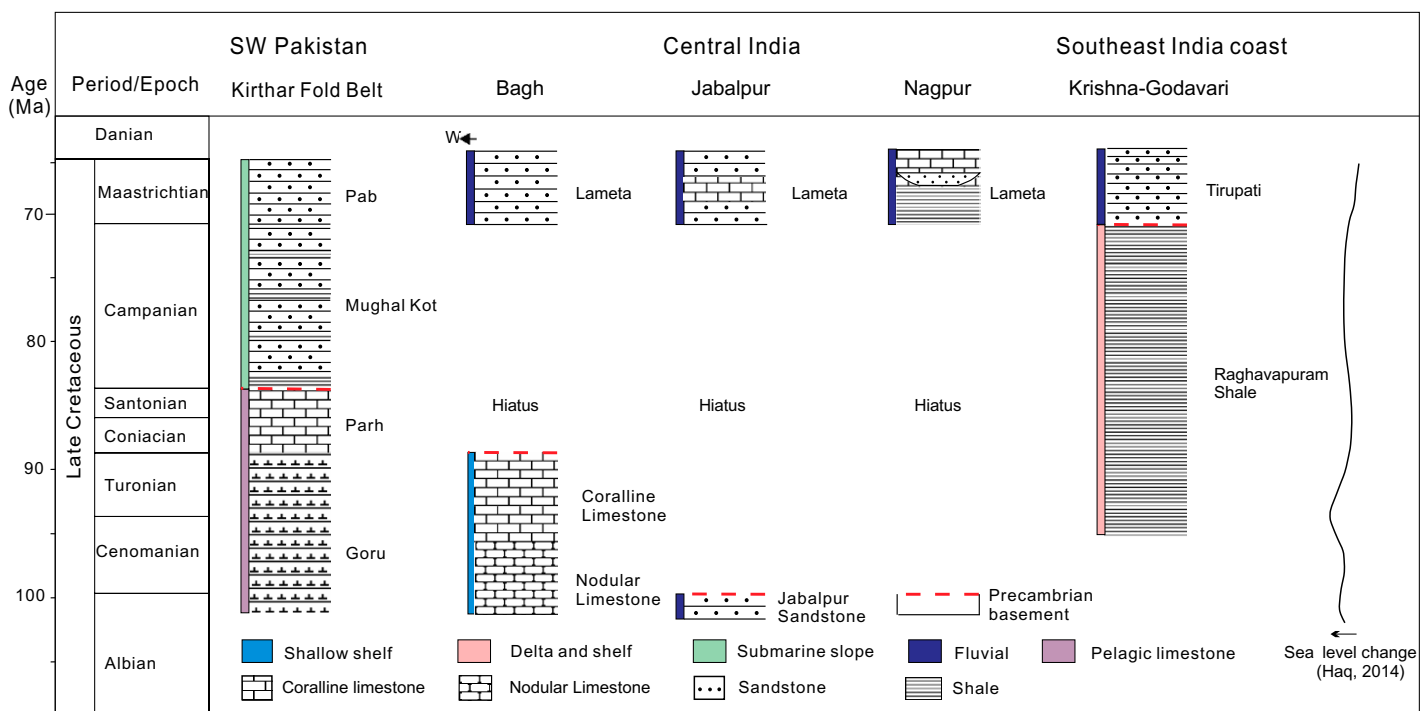


Figure 11. Stratigraphic correlation chart for Upper Cretaceous successions deposited in western Pakistan and peninsular India. Locations of the sections studied are indicated by yellow dots in Figure 1. Stratigraphic logs: Kirthar belt (modified from Smewing et al., 2002); Bagh, Jabalpur, and Nagpur areas in central India (modified from Tandon, 2000; Tripathi, 2006); Krishna-Godavari in eastern India (modified from Gupta, 2006).

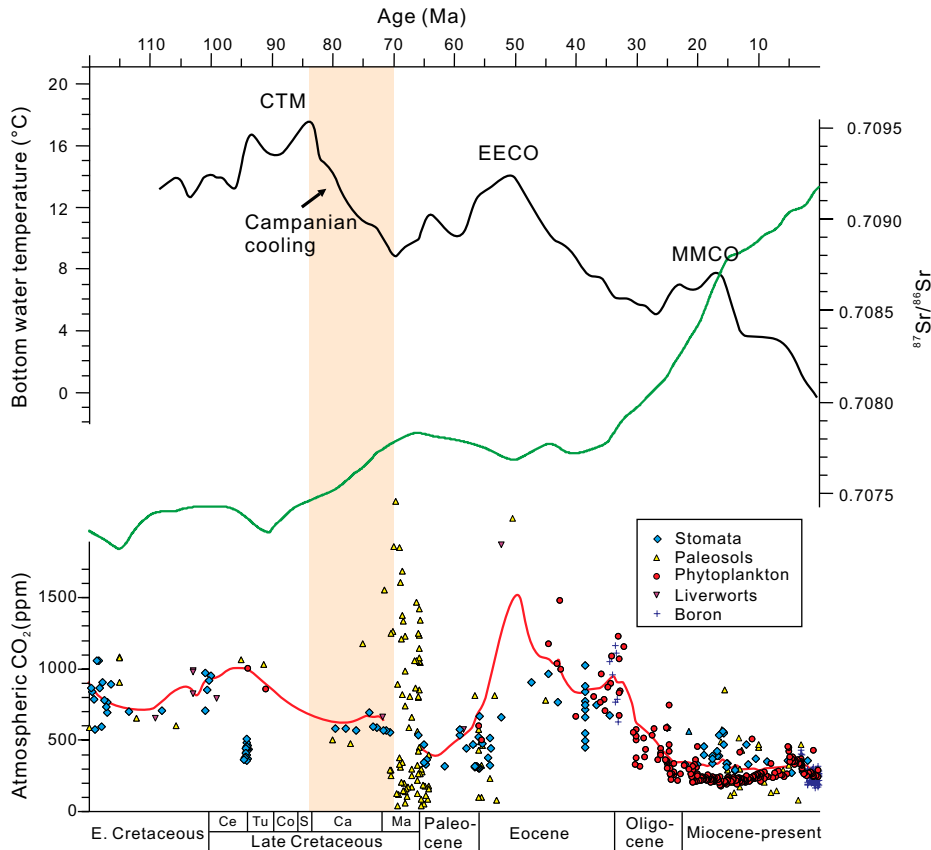


Figure 12. Water temperature shows cooling (Cramer et al., 2011), $^{87}\text{Sr}/^{86}\text{Sr}$ ratio shows increase of continental weathering (McArthur et al., 2001), and atmospheric $p\text{CO}_2$ estimated from various proxies shows declining of atmospheric $p\text{CO}_2$ in Campanian (Royer, 2010; Beerling and Royer, 2011; Zhang et al., 2018). CTM—Cretaceous thermal maximum; EECO—early Eocene climatic optimum; MMCO—middle Miocene climatic optimum; Ce—Cenomanian; Tu—Turonian; Co—Coniacian; S—Santonian; Ca—Campanian; Ma—Maastrichtian.

lapping onto the uplifted area, development of erosional unconformities, and radial paleo-flow directions recorded in sedimentary rocks (Cox, 1989; Rainbird and Ernst, 2001). The stratigraphic successions exposed in the Tethys Himalaya, in the Kirthar fold-and-thrust belt, and in central to southeastern India document a marked shallowing-upward depositional trend that characterizes Maastrichtian strata all around the core of peninsular India, just before the Deccan magmatic outburst around the Cretaceous-Tertiary boundary. Most of the Campanian is missing in the Tethys Himalaya, and a disconformity separates Santonian and Campanian strata in the Kirthar fold belt, and Campanian and Maastrichtian strata in the Krishna-Godavari Basin (Figs. 3 and 11). In the region closer to the central uplift, stratigraphic sections exhibit a more extensive and prolonged hiatus, which spans from the Coniacian to the early Maastrichtian

in the Bagh area and from the Cenomanian to the early Maastrichtian in the Jabalpur and Nagpur areas (Fig. 11). Thicker sediment accumulation and shorter periods of nondeposition in peripheral areas than in the central region, together with widespread shallowing-upward depositional trends, represent robust evidence of topographic uplift associated with Deccan magmatism.

Campanian Cooling Triggered by Surface Uplift?

There is general consensus that late Cenomanian to early Turonian times were characterized by the warmest climate of the last 100 m.y., with ice-free polar regions and tropical sea-surface temperatures higher than 35 °C. This warm period was followed by global cooling in the Campanian–Maastrichtian (Fig. 12), which coincided with declining atmospheric $p\text{CO}_2$

levels from ~1975 to ~450 ppm (Linnert et al., 2014; Wang et al., 2014). Silicate weathering on continents consumes and stabilizes Earth's atmospheric CO_2 , providing a negative feedback to maintain the homeostatic balance of the long-term ($\geq 10^5$ yr) carbon cycle (Gaillardet et al., 1999). Surface uplift associated with magmatic upwelling before the outburst of Deccan flood basalts, and consequently increased weathering rates, thus represents a viable causal mechanism for Campanian cooling. Surface uplift preceding major Deccan volcanism may have affected an area as large as 2000–2500 km in diameter situated in the warm-humid subequatorial belt (Umar et al., 2014). The present average CO_2 consumption rate is estimated at $\sim 5.7 \times 10^5$ mol km^{-2} yr^{-1} , based on geochemical data from the Narmada, Godavari, and Cauveri River waters (Gaillardet et al., 1999). Such estimated CO_2 -consumption rates by weathering of continental crust over an area as vast as that affected by surface uplift before Deccan volcanism must have contributed significantly to the global decline in atmospheric $p\text{CO}_2$ and consequent climate cooling in Campanian–Maastrichtian times.

CONCLUSIONS

The stratigraphic and microfacies analysis of marine carbonate successions exposed in the Tethys Himalaya of southern Tibet has revealed the existence of a major hiatus indicating a prolonged phase of nondeposition and surface uplift by ~100 m during Campanian times. Santonian strata documenting deep-marine outer-ramp environments are disconformably overlain by Maastrichtian middle-ramp to inner-ramp sediments documenting abrupt shallowing. Sediment bypass and starvation persisted for as much as 10 m.y.

The very same sedimentation pattern characterizes the Zanskar Range of the northwestern Himalaya, and a coeval hiatus and similar shallowing-upward trends are documented by sedimentary successions exposed in the Kirthar fold-and-thrust belt of western Pakistan and in peninsular India. These strata, deposited all around the core of peninsular India, record thicker sediment accumulation and shorter periods of nondeposition than in the main Deccan province closer to the center of the topographic dome. This represents evidence of surface uplift associated with magmatic upwelling at the base of the Indian lithosphere, which began in early Campanian times and eventually led to the outburst of Deccan continental flood basalts around the Cretaceous-Tertiary boundary. Topographic doming in the warm-humid subequatorial belt and associated silicate

weathering may have contributed to lowered levels of global atmospheric $p\text{CO}_2$ and climate cooling during the Campanian–Maastrichtian. This climatic event may have set the scene for the major faunal extinction that took place contemporaneously with the climax of Deccan volcanism at the end of the Mesozoic Era.

ACKNOWLEDGMENTS

We thank Gaoyuan Sun and Jiangang Wang for their assistance in the field. We are grateful to R.H. Rainbird and an anonymous reviewer for their helpful advice and constructive suggestions, and to Science Editor Brad Singer and Associate Editor Rajat Mazumder for their careful handling. This study was financially supported by the National Natural Science Funds for Distinguished Young Scholars (no. 41525007) and National Natural Science Funds of China (no. 41702105).

REFERENCES CITED

- Anderson, D.L., 2013, The persistent mantle plume myth: Australian Journal of Earth Sciences, v. 60, p. 657–673, <https://doi.org/10.1080/08120099.2013.835283>.
- Bansal, U., Banerjee, S., Ruidas, D.K., and Pande, K., 2018, Origin and geochemical characterization of the glauconites in the Upper Cretaceous Lameta Formation, Narmada Basin, central India: Journal of Palaeogeography, v. 7, p. 99–116, <https://doi.org/10.1016/j.jop.2017.12.001>.
- Beerling, D.J., and Royer, D., 2011, Convergent Cenozoic CO_2 history: Nature Geoscience, v. 4, p. 418–420, <https://doi.org/10.1038/ngeo1186>.
- Berggren, W.A., 1973, The Pliocene time scale: Calibration of planktonic foraminiferal and calcareous nannoplankton zones: Nature, v. 243, p. 391–397, <https://doi.org/10.1038/243391a0>.
- Berle, R.J., and Suttner, T.J., 2005, New biostratigraphic data for the Chikkim formation (Cretaceous, Tethyan Himalaya, India): Cretaceous Research, v. 26, no. 6, p. 882–894, <https://doi.org/10.1016/j.cretres.2005.06.001>.
- Blow, W.H., 1979, The Cainozoic Foraminifera: Leiden, Netherlands, E.J. Brill, 3 volumes, 1452 p.
- Boudagher-Fadel, M.K., 2013, Biostratigraphic and Geological Significance of Planktonic Foraminifera (2nd ed.): London, University College of London, 307 p.
- Boudagher-Fadel, M.K., Price, G.D., Hu, X., and Li, J., 2015, Late Cretaceous to early Paleogene foraminiferal biozones in the Tibetan Himalayas, and a pan-Tethyan foraminiferal correlation scheme: Stratigraphy, v. 12, p. 67–91.
- Bryan, S.E., and Ernst, R.E., 2008, Revised definition of large igneous provinces (LIPs): Earth-Science Reviews, v. 86, no. 1, p. 175–202, <https://doi.org/10.1016/j.earscirev.2007.08.008>.
- Campbell, I.H., and Griffiths, R.W., 1990, Implications of mantle plume structure for the evolution of flood basalts: Earth and Planetary Science Letters, v. 99, no. 1–2, p. 79–93, [https://doi.org/10.1016/0012-821X\(90\)90072-6](https://doi.org/10.1016/0012-821X(90)90072-6).
- Cox, K.G., 1989, The role of mantle plumes in the development of continental drainage patterns: Nature, v. 342, p. 873–877, <https://doi.org/10.1038/342873a0>.
- Cramer, B.S., Miller, K.G., Barrett, P.J., and Wright, J.D., 2011, Late Cretaceous–Neogene trends in deep ocean temperature and continental ice volume: Reconciling records of benthic foraminiferal geochemistry ($\delta^{18}\text{O}$ and Mg/Ca) with sea level history: Journal of Geophysical Research, v. 116, C12023, <https://doi.org/10.1029/2011JC007255>.
- DeCelles, P., Kapp, P., Gehrels, G., and Ding, L., 2014, Paleocene–Eocene foreland basin evolution in the Himalaya of southern Tibet and Nepal: Implications for the age of initial India–Asia collision: Tectonics, v. 33, no. 5, p. 824–849, <https://doi.org/10.1002/2014TC003522>.
- Dunham, R.J., 1962, Classification of carbonate rocks according to depositional textures, in Ham, W.E., ed., Classification of Carbonate Rocks: American Association of Petroleum Geologists Memoir 1, p. 108–121.
- Embray, A.F., and Klovon, J.E., 1971, A Late Devonian reef tract on northeastern Banks Island, NWT: Bulletin of Canadian Petroleum Geology, v. 19, p. 730–781.
- Flügel, E., 2010, Microfacies of Carbonate Rocks: Analysis, Interpretation and Application (2nd ed.): Berlin, Springer-Verlag, p. 721–722, <https://doi.org/10.1007/978-3-642-03796-2>.
- Gaillardet, J., Dupré, B., Allegrè, C.J., 1999, Geochemistry of large river suspended sediments: Silicate weathering or recycling tracer?: Geochimica et Cosmochimica Acta, v. 63, no. 23/24, p. 4037–4051, [https://doi.org/10.1016/S0016-7037\(99\)00307-5](https://doi.org/10.1016/S0016-7037(99)00307-5).
- Gansser, A., 1964, The Geology of the Himalayas: New York, Wiley Interscience, 289 p.
- Garzanti, E., 1993a, Himalayan ironstones, “superplumes,” and the breakup of Gondwana: Geology, v. 21, no. 2, p. 105–108, [https://doi.org/10.1130/0091-7613\(1993\)021<0105:HISATB>2.3.CO;2](https://doi.org/10.1130/0091-7613(1993)021<0105:HISATB>2.3.CO;2).
- Garzanti, E., 1993b, Sedimentary evolution and drowning of a passive margin shelf (Giumal Group; Zaskar Tethys Himalaya, India): Palaeoenvironmental changes during final break-up of Gondwanaland, in Treloar, P.J., and Searle, M.P., eds., Himalayan Tectonics: Geological Society [London] Special Publication 74, p. 277–298, <https://doi.org/10.1144/GSL.SP.1993.074.01.20>.
- Garzanti, E., and Hu, X., 2015, Latest Cretaceous Himalayan tectonics: Obduction, collision or Deccan-related uplift?: Gondwana Research, v. 28, no. 1, p. 165–178, <https://doi.org/10.1016/j.gr.2014.03.010>.
- Gradstein, F.M., Ogg, G., and Schmitz, M., 2012, The Geologic Time Scale: Boston, Massachusetts, Elsevier, 1176 p.
- Gunnell, Y., Gallagher, K., Carter, A., Widdowson, M., and Hurford, A.J., 2003, Denudation history of the continental margin of western peninsular India since the early Mesozoic—Reconciling apatite fission-track data with geomorphology: Earth and Planetary Science Letters, v. 215, p. 187–201, [https://doi.org/10.1016/S0012-821X\(03\)00380-7](https://doi.org/10.1016/S0012-821X(03)00380-7).
- Guo, T., Liang, D., Zhang, Y., and Zhao, C., 1991, Ali Geology: Wuhan, The China University of Geosciences Press, 464 p.
- Gupta, S.K., 2006, Basin architecture and petroleum system of Krishna Godavari Basin, east coast of India: The Leading Edge, v. 25, no. 7, p. 830–837, <https://doi.org/10.1190/1.2221360>.
- Halkett, A., White, N., Chandra, K., and Lal, N.K., 2001, Dynamic uplift of the Indian peninsula and the Réunion plume: San Francisco, California, American Geophysical Union, Fall Meeting, abstract T11A-0845.
- Haq, B.U., 2014, Cretaceous eustasy revisited: Global and Planetary Change, v. 113, no. 2, p. 44–58, <https://doi.org/10.1016/j.gloplacha.2013.12.007>.
- Hu, X., Jansa, L., Chen, L., Griffin, W.L., O’Reilly, S.Y., and Wang, J., 2010, Provenance of Lower Cretaceous Wölong volcanics in the Tibetan Tethyan Himalaya: Implications for the final breakup of eastern Gondwana: Sedimentary Geology, v. 223, no. 3, p. 193–205, <https://doi.org/10.1016/j.sedgeo.2009.11.008>.
- Hu, X., Garzanti, E., Wang, J., Huang, W., An, W., and Webb, A., 2016, The timing of India–Asia collision onset—Facts, theories, controversies: Earth-Science Reviews, v. 160, p. 264–299, <https://doi.org/10.1016/j.earscirev.2016.07.014>.
- Hu, X.M., Wang, C.S., Li, X.H., and Chen, L., 2006, Sedimentary facies of uppermost Jurassic and Lower Cretaceous in Guocuo area, southern Tibet: Journal of Paleogeography, v. 8, no. 2, p. 175–186.
- Hu, X.M., Hugh, D.S., Wang, J.G., Jiang, H.H., and Wu, F.Y., 2012, Late Cretaceous–Paleogene stratigraphic and basin evolution in the Zhepure Mountain of southern Tibet: Implications for the timing of India–Asia initial collision: Basin Research, v. 24, no. 5, p. 520–543, <https://doi.org/10.1111/j.1365-2117.2012.00543.x>.
- Hu, X.M., Li, J., An, W., and Wang, J.G., 2017, The redefinition of Cretaceous–Paleogene lithostratigraphic units and tectonostratigraphic division in southern Tibet: Earth Science Frontiers, v. 24, no. 1, p. 174–194.
- Huang, W., Hinsbergen, D.J.J.V., Dekkers, M.J., Garzanti, E., Dupont-Nivet, G., Lippert, P.C., et al. et al., 2015, Paleolatitudes of the Tibetan Himalaya from primary and secondary magnetizations of Jurassic to Lower Cretaceous sedimentary rocks: Geochemistry Geophysics Geosystems, v. 16, no. 1, p. 77–100, <https://doi.org/10.1002/2014GC005624>.
- Jadoul, F., Berra, F., and Garzanti, E., 1998, The Tethys Himalayan passive margin from Late Triassic to Early Cretaceous (south Tibet): Journal of Asian Earth Sciences, v. 16, p. 173–194, [https://doi.org/10.1016/S0743-9547\(98\)00013-0](https://doi.org/10.1016/S0743-9547(98)00013-0).
- Jay, A.E., and Widdowson, M., 2008, Stratigraphy, structure and volcanology of the Deccan continental flood basalt province: Implications for eruptive extent and volumes: Journal of the Geological Society [London], v. 165, no. 1, p. 177–188, <https://doi.org/10.1144/0016-76492006-062>.
- Jerram, D.A., and Widdowson, M., 2005, The anatomy of continental flood basalt provinces: Geological constraints on the processes and products of flood volcanism: Lithos, v. 79, no. 3, p. 385–405, <https://doi.org/10.1016/j.lithos.2004.09.009>.
- Kassi, A.M., Kelling, G., Kasi, A.K., Umar, M., and Khan, A.S., 2009, Contrasting Late Cretaceous–Palaeocene lithostratigraphic successions across the Bibai thrust, western Sulaiman fold-thrust belt, Pakistan: Their significance in deciphering the early-collisional history of the NW Indian plate margin: Journal of Asian Earth Sciences, v. 35, no. 5, p. 435–444, <https://doi.org/10.1016/j.jseas.2009.02.006>.
- Kazmi, A.H., and Abbasi, I.A., 2008, Stratigraphy and Historical Geology of Pakistan: Peshawar, Pakistan, Department and National Centre of Excellence in Geology, University of Peshawar, 524 p.
- Leckie, R.M., 1987, Paleocology of mid-Cretaceous planktonic foraminifera: A comparison of open ocean and epicontinental sea assemblages: Micropaleontology, v. 33, no. 2, p. 164–176, <https://doi.org/10.2307/1485491>.
- Li, G., Jiang, G., Hu, X., and Wan, X., 2009, New biostratigraphic data from the Cretaceous Bolinxiala Formation in Zanda, southwestern Tibet of China, and their paleogeographic and paleoceanographic implications: Cretaceous Research, v. 30, no. 4, p. 1005–1018, <https://doi.org/10.1016/j.cretres.2009.03.005>.
- Linnert, C., Robinson, S.A., Lees, J.A., Bown, P.R., Pérez-Rodríguez, I., Petrizzo, M.R., Falzoni, F., Littler, K., Arz, J.A., and Russell, E.E., 2014, Evidence for global cooling in the Late Cretaceous: Nature Communications, v. 5, p. 4194, <https://doi.org/10.1038/ncomms5194>.
- Manmohan, M., Rao, M.R.R., Kamaraju, A.V.V.S., and Yalamarty, S.S., 2003, Origin and occurrence of Lower Cretaceous high gamma–high resistivity (Raghavapuram) shale—A key stratigraphic sequence for hydrocarbon exploration in Krishna–Godavari basin, A.P.: Journal of the Geological Society of India, v. 62, p. 271–289.
- McArthur, J.M., Howarth, R.J. and Bailey, T.R., 2001, Strontium isotope stratigraphy: LOWESS version 3: Best fit to the marine Sr-isotope curve for 0–509 Ma and accompanying look-up table for deriving numerical age: The Journal of Geology, v. 109, no. 2, p. 155–170, <https://doi.org/10.1086/319243>.
- Mount, J., 1985, Mixed siliciclastic and carbonate sediments: A proposed first-order textural and compositional classification: Sedimentology, v. 32, p. 435–442, <https://doi.org/10.1111/j.1365-3091.1985.tb00522.x>.
- Nicora, A., Garzanti, E., and Fois, E., 1987, Evolution of the Tethys Himalaya continental shelf during Maastrichtian to Paleocene (Zaskar, India): Rivista Italiana di Paleontologia e Stratigrafia, v. 92, p. 439–496.
- Pan, G.T., Ding, J., Yao, D., and Wang, L., 2004, The Guide Book of Geologic Map of the Qinghai–Xizang (Tibet) Plateau and Adjacent Areas: Chengdu, China, Chengdu Cartographic Publishing House, scale 1:1,500,000 [in Chinese with English abstract].
- Premoli Silva, I., and Sliter, W.V., 1999, Cretaceous paleoceanography: Evidence from planktonic foraminiferal evolution, in Barrera, E., and Johnson, C.C., eds., The Evolution of Cretaceous Ocean–Climatic System: Geological Society of America Special Paper 332, p. 301–328, <https://doi.org/10.1130/0-8137-2332-9.301>.
- Premoli Silva, I., and Verga, D., 2004, Practical manual of Cretaceous planktonic foraminifera, in Verga, D., and

- Rettori, R., eds., International School on Planktonic Foraminifera Course: Cretaceous: Perugia, Italy, Universities of Perugia and Milan, Tipografia Pontefelcino, p. 283.
- Premoli Silva, I., Garzanti, E., and Gaetani, M., 1991, Stratigraphy of the Chikkim and Fatu la formations in the Zangla and Zumlung units (Zanskar Range, India) with comparisons to the Thakkhola region (central Nepal): Mid-Cretaceous evolution of the Indian passive margin: *Rivista Italiana di Paleontologia e Stratigrafia*, v. 97, no. 3, p. 511–564.
- Rainbird, R.H., and Ernst, R.E., 2001, The sedimentary record of mantle-plume uplift, in Ernst, R.E., and Buchan, K.L., eds., *Mantle Plumes: Their Identification through Time*: Geological Society of America Special Paper 352, p. 227–245.
- Rao, G.N., 2001, Sedimentation, stratigraphy, and petroleum potential of Krishna-Godavari Basin, east coast of India: *American Association of Petroleum Geologists Bulletin*, v. 85, no. 9, p. 1623–1643.
- Ratschbacher, L., Frisch, W., Liu, G., and Chen, C., 1994, Distributed deformation in southern and western Tibet during and after the India-Asia collision: *Journal of Geophysical Research*, v. 99, p. 19,917–19,945, <https://doi.org/10.1029/94JB00932>.
- Royer, D.L., 2010, Fossil soils constrain ancient climate sensitivity: *Proceedings of the National Academy of Sciences of the United States of America*, v. 107, no. 2, p. 517–518, <https://doi.org/10.1073/pnas.0913188107>.
- Sahu, H.S., Raab, M.J., Kohn, B.P., Gleadow, A.J., and Kumar, D., 2013, Denudation history of the eastern Indian peninsula from apatite fission track analysis: Linking possible plume-related uplift and the sedimentary record: *Tectonophysics*, v. 608, p. 1413–1428, <https://doi.org/10.1016/j.tecto.2013.06.002>.
- Saunders, A.D., Jones, S.M., Morgan, L.A., Pierce, K.L., Widdowson, M., and Xu, Y., 2007, Regional uplift associated with continental large igneous provinces: The roles of mantle plumes and the lithosphere: *Chemical Geology*, v. 241, p. 282–318, <https://doi.org/10.1016/j.chemgeo.2007.01.017>.
- Sciunnach, D., and Garzanti, E., 2012, Subsidence history of the Tethys Himalaya: *Earth-Science Reviews*, v. 111, no. 1–2, p. 179–198.
- Searle, M.P., and Godin, L., 2003, The South Tibetan detachment and the Manaslu Leucogranite: A structural reinterpretation and restoration of the Annapurna-Manaslu Himalaya, Nepal: *The Journal of Geology*, v. 111, no. 5, p. 505–523, <https://doi.org/10.1086/376763>.
- Sharma, K.K., 2007, K-T magmatism and basin tectonism in western Rajasthan, India, results from extensional tectonics and not from Réunion plume activity, in Foulger, G.R., and Jurdy, D.M., eds., *Plates, Plumes and Planetary Processes*: Geological Society of America Special Paper 430, p. 775–784, [https://doi.org/10.1130/2007.2430\(35\)](https://doi.org/10.1130/2007.2430(35)).
- Sheth, H.C., 2007, Plume-related regional prevolcanic uplift in the Deccan Traps: Absence of evidence, evidence of absence, in Foulger, G.R., and Jurdy, D.M., eds., *Plates, Plumes and Planetary Processes*: Geological Society of America Special Paper 430, p. 785–813.
- Smewing, J.D., Warburton, J., Daley, T., Copestake, P., and Ulhaq, N., 2002, Sequence stratigraphy of the southern Kirthar fold belt and middle Indus Basin, Pakistan, in Clift, P.D., Kroon, D., Gaedicke, C., and Craig, J., eds., *The Tectonic and Climatic Evolution of the Arabian Sea Region*: Geological Society [London] Special Publication 195, p. 273–299, <https://doi.org/10.1144/GSL.SP.2002.195.01.15>.
- Srivastava, A.K., and Mankar, R.S., 2015, Lithofacies architecture and depositional environment of Late Cretaceous Lameta formation, central India: *Arabian Journal of Geosciences*, v. 8, no. 1, p. 207–226, <https://doi.org/10.1007/s12517-013-1192-y>.
- Stampfli, G.M., and Borel, G.D., 2002, A plate tectonic model for the Paleozoic and Mesozoic constrained by dynamic plate boundaries and restored synthetic oceanic isochrones: *Earth and Planetary Science Letters*, v. 196, no. 1–2, p. 17–33, [https://doi.org/10.1016/S0012-821X\(01\)00588-X](https://doi.org/10.1016/S0012-821X(01)00588-X).
- Tandon, S.K., 2000, Spatio-temporal patterns of environmental changes in Late Cretaceous sequences of central India, in Okada, H., and Mateer, N.J., eds., *Cretaceous Environments of Asia*: Amsterdam, Netherlands, Elsevier, *Developments in Palaeontology and Stratigraphy* 17, p. 225–241.
- Tandon, S.K., 2002, Records of the influence of Deccan volcanism on contemporary sedimentary environments in central India: *Sedimentary Geology*, v. 147, no. 1, p. 177–192, [https://doi.org/10.1016/S0037-0738\(01\)00196-8](https://doi.org/10.1016/S0037-0738(01)00196-8).
- Tripathi, S.C., 2006, Geology and evolution of the Cretaceous infratrappean basins of lower Narmada valley, western India: *Journal of the Geological Society of India*, v. 67, p. 459–468.
- Umar, M., Khan, A.S., Kelling, G., and Kassi, A.M., 2011, Depositional environments of Campanian–Maastrichtian successions in the Kirthar fold belt, southwest Pakistan: Tectonic influences on Late Cretaceous sedimentation across the Indian passive margin: *Sedimentary Geology*, v. 237, no. 1, p. 30–45, <https://doi.org/10.1016/j.sedgeo.2011.02.001>.
- Umar, M., Friis, H., Khan, A.S., Kelling, G., Kassi, A.M., Sabir, M.A., et al. et al., 2014, Sediment composition and provenance of the Pab formation, Kirthar fold belt, Pakistan: Signatures of hot spot volcanism, source area weathering, and paleogeography on the western passive margin of the Indian plate during the Late Cretaceous: *Arabian Journal for Science and Engineering*, v. 39, no. 1, p. 311–324, <https://doi.org/10.1007/s13369-013-0850-4>.
- Wade, P., Paul, N.P., William, A., and Pälke, H., 2011, Review and revision of Cenozoic tropical planktonic foraminiferal biostratigraphy and calibration to the geomagnetic polarity and astronomical time scale: *Earth-Science Reviews*, v. 104, no. 1, p. 111–142, <https://doi.org/10.1016/j.earscirev.2010.09.003>.
- Wan, X.Q., Jansa, L.F., and Sarti, M., 2002, Cretaceous and Paleogene boundary strata in southern Tibet and their implication for the India-Eurasia collision: *Lethaia*, v. 35, p. 131–146, <https://doi.org/10.1080/002411602320183999>.
- Wang, Y., Huang, C., Sun, B., Quan, C., Wu, J., and Lin, Z., 2014, Paleo-CO₂ variation trends and the Cretaceous greenhouse climate: *Earth-Science Reviews*, v. 129, p. 136–147, <https://doi.org/10.1016/j.earscirev.2013.11.001>.
- Wendler, I., Wendler, J., Gräfe, K.U., Lehmann, J., and Willems, H., 2009, Turonian to Santonian carbon isotope data from the Tethys Himalaya, southern Tibet: *Cretaceous Research*, v. 30, no. 4, p. 961–979, <https://doi.org/10.1016/j.cretres.2009.02.010>.
- Wendler, J., Gräfe, K.U., and Willems, H., 2002, Palaeoecology of calcareous dinoflagellate cysts in the mid-Cenomanian boreal realm: Implications for the reconstruction of palaeoceanography of the NW European shelf sea: *Cretaceous Research*, v. 23, no. 2, p. 213–229, <https://doi.org/10.1006/cres.2002.0311>.
- White, R., and McKenzie, D., 1989, Magmatism at rift zones: The generation of volcanic continental margins and flood basalts: *Journal of Geophysical Research–Solid Earth*, v. 94, no. B6, p. 7685–7729, <https://doi.org/10.1029/JB094iB06p07685>.
- Willems, H., and Zhang, B.G., 1993, Cretaceous and Lower Tertiary sediments of Tethys Himalaya in the area of Gamba (south Tibet, PR China), in Willems, H., ed., *Geoscientific Investigations in the Tethyan Himalayas: Berichte aus Fachbereich Geowissenschaften der Universität Bremen*, v. 38, p. 3–27.
- Willems, H., Zhou, Z., Zhang, B., and Gräfe, K.U., 1996, Stratigraphy of the Upper Cretaceous and Lower Tertiary strata in the Tethyan Himalayas of Tibet (Tingri area, China): *Geologische Rundschau*, v. 85, p. 723–754, <https://doi.org/10.1007/BF02440107>.
- Wilson, J.L., 1975, *Carbonate Facies in Geologic Time*: New York, Springer-Verlag, 471 p., <https://doi.org/10.1007/978-1-4612-6383-8>.
- Wu, C., Shi, Y.K., and Hu, X.M., 2011, The disconformity in the Late Cretaceous strata at Tingri (southern Tibet) and its age constrained by planktonic foraminifera: *Acta Micropalaeontologica Sinica*, v. 28, p. 381–401.
- Wu, F.Y., Ji, W.Q., Wang, J.G., Liu, C.Z., Chung, S.L., and Clift, P.D., 2014, Zircon U-Pb and Hf isotopic constraints on the onset time of India-Asia collision: *American Journal of Science*, v. 314, no. 2, p. 548–579, <https://doi.org/10.2475/02.2014.04>.
- Yu, G.M., Xu, Y.L., Zhang, Q.H., et al. et al., 1983, Subdivision and correlation of Jurassic system in the Nyalam area, Xizang (Tibet), in CGQXP Editorial Committee, Ministry of Geology and Mineral Resources PRC, ed., *Contribution to the Geology of the Qinghai Xizang (Tibet) Plateau*: Beijing, Geological Publishing House, v. 11, p. 165–176.
- Zhang, L.M., Wang, C.S., Wignall, B.P., Kluge, T., Wan, X.Q., Wang, Q., and Gao, Y., 2018, Deccan volcanism caused coupled pCO₂ and terrestrial temperature rises, and pre-impact extinctions in northern China: *Geology*, v. 46, no. 3, p. 271–274, <https://doi.org/10.1130/G39992.1>.

SCIENCE EDITOR: BRADLEY S. SINGER
ASSOCIATE EDITOR: RAJAT MAZUMDER

MANUSCRIPT RECEIVED 5 SEPTEMBER 2018
REVISED MANUSCRIPT RECEIVED 18 APRIL 2019
MANUSCRIPT ACCEPTED 13 JUNE 2019

Printed in the USA